

## Tides in the Sea of Okhotsk

ZYGMUNT KOWALIK AND IGOR POLYAKOV

*Institute of Marine Science, University of Alaska, Fairbanks, Alaska*

(Manuscript received 8 October 1996, in final form 25 August 1997)

### ABSTRACT

Eight major tidal constituents in the Sea of Okhotsk have been investigated using a numerical solution of tidal equations on a  $5'$  space grid. The tides are dominated by the diurnal constituents. Diurnal tidal currents are enhanced in Shelikhov Bay and Penzhinskaya Guba, at Kashevarov Bank, in proximity to the Kuril Islands and at a few smaller locations. The major energy sink for diurnal tides (over 60% of the total energy) is Shelikhov Bay and Penzhinskaya Guba. The major portion of semidiurnal tide energy is dissipated in the northwestern region of the Sea of Okhotsk and in Shelikhov Bay and Penzhinskaya Guba. Nonlinear interactions of diurnal currents are investigated through  $K_1$  and  $O_1$  constituent behavior over Kashevarov Bank. These interactions generate residual circulation of the order of  $10 \text{ cm s}^{-1}$ , major oscillations at semidiurnal and fortnightly periods (13.66 days), and higher harmonics of basic tidal periods. The  $M_2$  tidal current, caused by the nonlinear interaction of the diurnal constituents over Kashevarov Bank, constitutes approximately a half of the total  $M_2$  tide current there. The fortnightly current, through nonlinear interactions, also influences basic diurnal tidal currents by inducing fortnightly variations in the amplitude of these currents.

### 1. Introduction

The Sea of Okhotsk (SO) is a region of large tidal sea-level oscillations and strong tidal currents. In shallow Penzhinskaya Guba, total tidal sea level oscillations reach 13 m. Because of the strong currents and sea level changes, the tides significantly influence water mass formation in the SO. Total tidal currents of up to 4 knots occur in the Kuril Straits (Leonov 1960). These large currents cause mixing of the upper-ocean layer around the Kuril Islands, generating a front between the Sea of Okhotsk and the Pacific Ocean (Gladyshev 1995). Kitani and Shimazaki (1971) found an almost homogeneous vertical structure of the temperature, salinity, and dissolved oxygen over Kashevarov Bank and on the shelf in the mouth of Penzhinskaya Guba. During winter, strong vertical mixing sustains a polynya over Kashevarov Bank. According to Alfultis and Martin (1987), to maintain this polynya a vertical heat flux of  $50\text{--}100 \text{ W m}^{-2}$  is necessary. One source of this vertical mixing is a strong tidal current.

Enhanced tidal currents in both the semidiurnal and diurnal bands usually occur in shallow areas due to topographic amplification. In the diurnal band of oscillations the maximum current can also be associated with the occurrence of shelf waves. Enhanced velocity along the shelf break and over isolated seamounts (see sum-

mary by Foreman et al. 1995) is caused by near-resonant amplification of diurnal currents by topography. Investigations of the resonance band of frequencies over seamounts by Chapman (1983, 1989), Brink (1989), Hunkins (1986), and Haidvogel et al. (1993) delineated the dependence of trapped waves on the range of topographic sizes and stratification. From their results one can conclude that regions of local resonance are more likely to be found in the polar oceans, where large values of the Coriolis parameter occur.

There are at least two regions of well-defined tidally generated topographic waves in the SO: off Hokkaido Island and along Sakhalin Island. Investigations of tidal current and sea level at the northern coast off Hokkaido Island and in Soya Strait by Aota and Matsuyama (1987) and Odamaki (1994) reveal that the differences in tidal phase and amplitude between the Sea of Okhotsk and the Sea of Japan result in strong diurnal currents at Soya Strait. Odamaki (1994) demonstrated that these strong currents generate a shelf wave along the coast of Hokkaido. Aota and Matsuyama (1987) carried out an analysis of a 32-month current data series from the mooring station near Soya Strait and observed a high temporal variability of the tidal current harmonic constants.

Strong diurnal currents were also observed by Rabinovich and Zhukov (1984) along the coast of Sakhalin. Their data were compared against an analytical model that describes the barotropic shelf wave and Kelvin wave (Yefimov et al. 1985). Computations showed that tidal currents are controlled by the first mode of the barotropic shelf wave, whereas sea level is related to

---

*Corresponding author address:* Dr. Zygmunt Kowalik, Institute of Marine Science, University of Alaska, Fairbanks, AK 99775-7220.  
E-mail: ffzk@tide.ims.alaska.edu

both the shelf and Kelvin waves. Superposition of the shelf wave and Kelvin wave results in a set of amphidromic points along the coast of Sakhalin Island.

Suzuki and Kanari (1986) developed a tidal model of the Okhotsk Sea with a resolution of 18.4 km. Rather high spatial resolution allowed the determination of trapped tidal energy in the diurnal band of oscillations not only off Sakhalin but also above Kashevarov Bank and in the Kuril Islands region. In the latter region shelf wave dynamics was demonstrated by Yefimov et al. (1985) through direct measurements and theory.

In this study we shall compute eight dominant tidal constituents using a high spatial resolution. Analysis of computed sea level and currents is aimed primarily at describing regions of enhanced currents and patterns of energy flow in the entire SO. The focus of this study is investigation of mechanisms of tidal current enhancement over Kashevarov Bank, an area where two strong diurnal components,  $O_1$  and  $K_1$ , interact nonlinearly, resulting in semidiurnal and fortnightly periods and higher harmonics of the basic tidal periods.

## 2. Tidal equations and parameters

To obtain the distribution of tides in the SO we shall use the vertically averaged equations of motion and continuity in a spherical coordinate system (Gill 1982):

$$\frac{\partial u}{\partial t} + \frac{u}{R \cos \phi} \frac{\partial u}{\partial \lambda} + \frac{v}{R} \frac{\partial u}{\partial \phi} - f v - \frac{uv \sin \phi}{R \cos \phi} = -\frac{g}{R \cos \phi} \frac{\partial}{\partial \lambda} (\alpha \zeta - \beta \zeta_0) - \frac{\tau_\lambda^b}{\rho H} + Au \quad (1)$$

$$\frac{\partial v}{\partial t} + \frac{u}{R \cos \phi} \frac{\partial v}{\partial \lambda} + \frac{v}{R} \frac{\partial v}{\partial \phi} + f u + \frac{uv \sin \phi}{R \cos \phi} = -\frac{g}{R} \frac{\partial}{\partial \phi} (\alpha \zeta - \beta \zeta_0) - \frac{\tau_\phi^b}{\rho H} + Av \quad (2)$$

$$\frac{\partial \zeta}{\partial t} + \frac{1}{R \cos \phi} \frac{\partial (Hu)}{\partial \lambda} + \frac{1}{R \cos \phi} \frac{\partial}{\partial \phi} (Hv \cos \phi) = 0. \quad (3)$$

The operator  $A$  in the horizontal friction term in (1) and (2) is

$$A = N_h \left[ \frac{1}{R^2 \cos^2 \phi} \frac{\partial^2}{\partial \lambda^2} + \frac{1}{R^2 \cos \phi} \frac{\partial}{\partial \phi} \left( \cos \phi \frac{\partial}{\partial \phi} \right) \right]. \quad (4)$$

The bottom stress components are taken as

$$\tau_\lambda^b = \rho r u \sqrt{u^2 + v^2}; \quad \tau_\phi^b = \rho r v \sqrt{u^2 + v^2}. \quad (5)$$

In (5)  $r$  denotes the bottom drag coefficient; it will be taken as  $r = 2.6 \times 10^{-3}$ .

The following notation has been used in the above equations:  $\lambda$  and  $\phi$  denote longitude and latitude,  $t$  is time,  $\zeta$  is free surface elevation,  $u$  and  $v$  are velocity components along longitude and latitude respectively,  $\rho$  is water density,  $N_h$  is horizontal eddy viscosity ( $= 2.5 \times 10^6 \text{ cm}^2 \text{ s}^{-1}$ ),  $H$  denotes depth (it does not include

sea level),  $f$  is the Coriolis parameter,  $g$  denotes gravity acceleration,  $R$  is the radius of the earth,  $\zeta_0$  denotes the equilibrium tide, and  $\alpha$  and  $\beta$  are parameters accounting for tidal potential perturbations. The above value of the horizontal eddy viscosity  $N_h$  is required to preserve numerical stability.

Tidal forcing is described in (1) and (2) through the terms that are multiplied by coefficients  $\alpha$  and  $\beta$ . These terms include the tide-generating potential, but they also contain various corrections due to earth tide and ocean loading (Schwiderski 1979, 1981a–g). Coefficient  $\alpha$  defines ocean loading; its value ranges from 0.940 to 0.953 according to Ray and Sanchez (1989). A higher-order correction for the loading effect can be implemented as well (e.g., Francis and Mazzega 1990). The term  $\beta \zeta_0$  includes both the tide-generating potential and correction due to the earth tide. It is usually expressed as (Hendershott 1977)

$$\beta \zeta_0 = (1 + k - h) \zeta_0. \quad (6)$$

Here  $k$  and  $h$  denote Love numbers, which are equal to 0.302 and 0.602, respectively. These numbers are averaged over all tidal constituents. Expressions for the equilibrium tides  $\zeta_0$  are given by Schwiderski (1979, 1981a–g).

In the ensuing computations one additional simplification is introduced. Because the SO is only partly covered by pack ice in winter and its effect on tides is usually quite small (e.g., Kowalik 1981), the influence of pack ice is neglected.

## 3. Results of computation

The model domain is shown in Fig. 1. The location of the open boundary is marked by the double line. The domain includes the Sea of Okhotsk, the northern part of the Sea of Japan, and a small portion of the Pacific Ocean.

The SO is bounded by Hokkaido, the Kuril Islands, the Kamchatka Peninsula, Siberia, and Sakhalin Island (Fig. 1). The two major domains of the sea are a broad shelf area along the Siberian coast and a relatively flat central basin with depths of approximately 1000–1500 m. The Kuril Basin is the deepest region with depths of 3000 to 3200 m. For numerical solution of the tidal equations a spatial grid of 5' was applied. Boundary conditions at the open boundaries are specified by the sea level oscillations. The tidal constants for the eight major constituents at the Pacific Ocean open boundary are taken from Schwiderski's computations (Schwiderski 1979, 1981a–g). The spatial resolution of these data is 1°. The missing values for the 5' grid resolution were obtained by linear interpolation of Schwiderski's results. The Schwiderski data compare well with satellite data (Cartwright et al. 1991) and with recent world tide models by LeProvost et al. (1994) and Kantha (1995).

The mixed tide (eight constituents) was computed for

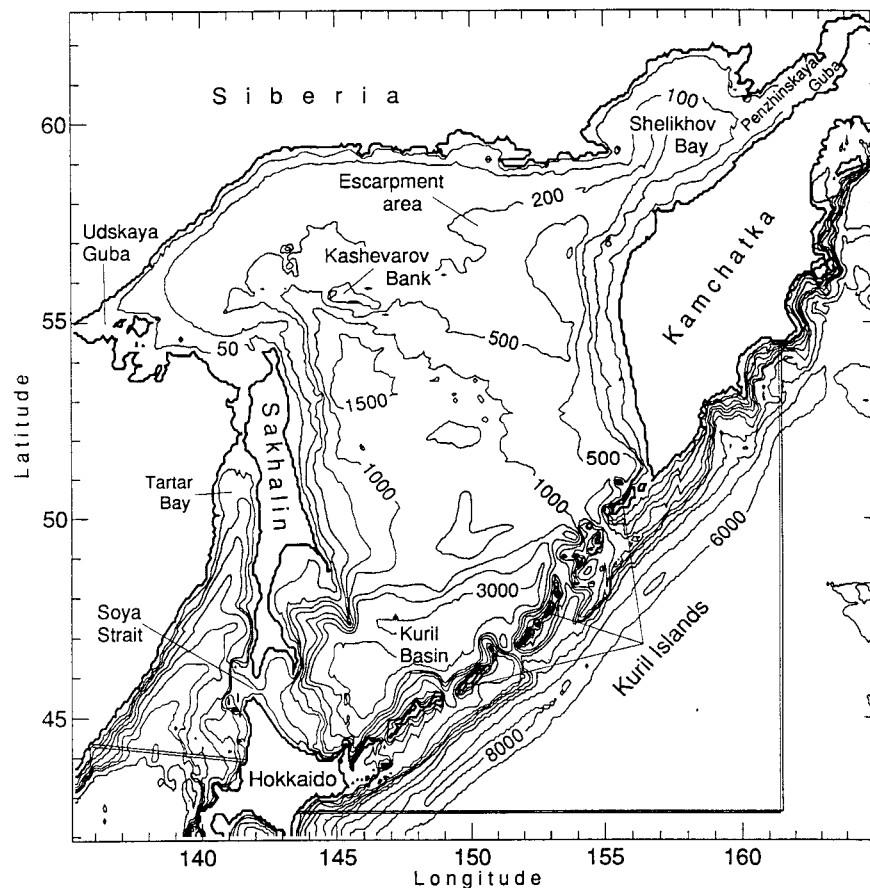


FIG. 1. Bathymetry of the Sea of Okhotsk. The double line denotes the open boundaries.

a two-month period. During the second month, when the total energy of the system became stationary, sea level and velocity were recorded hourly at each point of the domain. The standard for tidal harmonic analysis is a 29-day-long series with one-hour sampling (Foreman et al. 1995). The same approach was applied to investigate the tides over Kashevarov Bank, but for simplicity of analysis the mixed tide was represented by two major tidal constituents,  $K_1$  and  $O_1$ . In the latter experiment, the tide was computed for a four-month period, and sea level and currents were recorded hourly at each point of the domain during the last three months of the computation. The  $P_1$  and  $K_2$  harmonic constants were extracted from the record using an inference method described by Foreman et al. (1995). Additionally, results obtained for the  $P_1$  constituent from the computation of eight constituents were compared against  $P_1$  computed alone without interaction with the remaining constituents.

Cotidal charts for four major constituents,  $K_1$ ,  $O_1$ ,  $M_2$ , and  $S_2$ , are given in Figs. 2–5. Coamplitudes (cm) and cophases (deg) referred to Greenwich are shown by solid and dashed lines, respectively. The  $S_2$ ,  $N_2$ , and  $K_2$  constituent charts (the latter two not shown) generally repeat the pattern of the dominant  $M_2$  tidal constituent,

whereas the diurnal  $O_1$ ,  $P_1$ , and  $Q_1$  constituents (the latter two not shown as well) repeat the pattern of  $K_1$ , the dominant diurnal constituent.

Amplitudes of the diurnal constituents are large in the northeastern part of the SO. In the narrow Penzhinskaya Guba the  $K_1$  and  $O_1$  constituents have maximum amplitudes of approximately 2.5 and 1.5 m, respectively. The amplitude of the semidiurnal constituent  $M_2$  is only 1.3 m there. Along the southern and central Kamchatka coast the amplitudes of the diurnal constituents are slightly larger than those of semidiurnal constituents.

The largest calculated amplitudes for the semidiurnal band occur in Udskeya Guba. For example, amplitude of the  $M_2$  constituent is 1.81 m there. Diurnal tides are relatively weak in this bay (up to 0.6 m for the  $K_1$  constituent). Semidiurnal tides prevail along the Siberian coast, with amplitudes up to 1.3 and 0.52 m for the  $M_2$  and  $S_2$  constituents, respectively. However, the largest amplitudes of the diurnal constituents are in the range of 0.4–0.6 m along this coast.

Model results were verified by sea level observations from 108 stations of the SO and northern part of the Sea of Japan. Unfortunately, along the Siberian coast and Kamchatka Peninsula only 10 tide stations are available. The remaining 98 stations are located along the

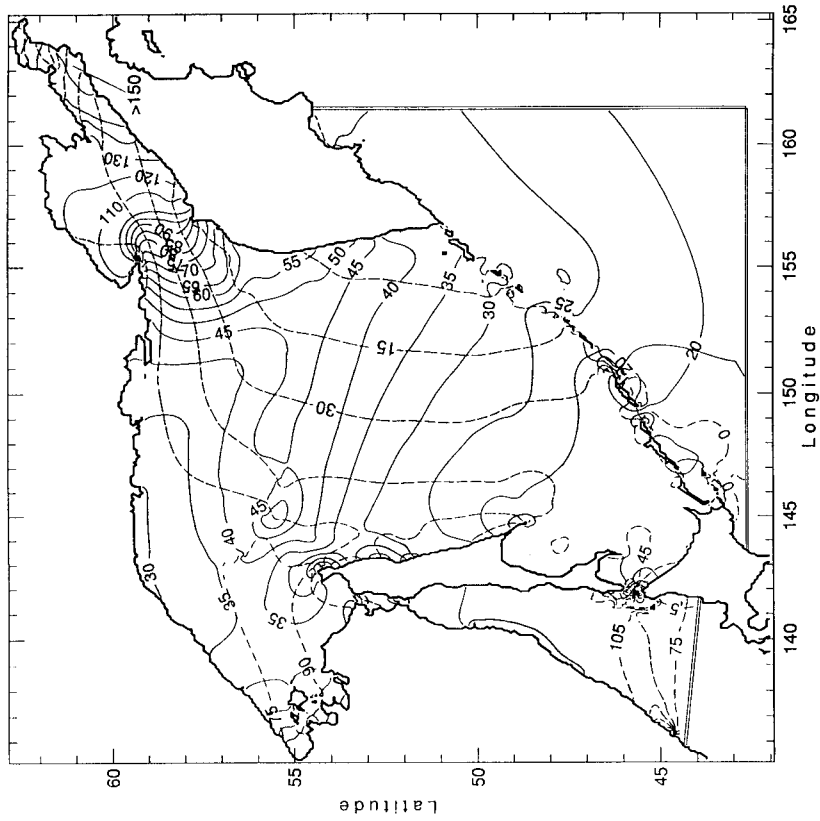


FIG. 3. Computed amplitudes (solid lines, cm) and phases (dashed lines, degrees) of surface elevation for the diurnal  $O_1$  tide. The phases are referred to Greenwich; the phase contours are plotted every  $15^\circ$ .

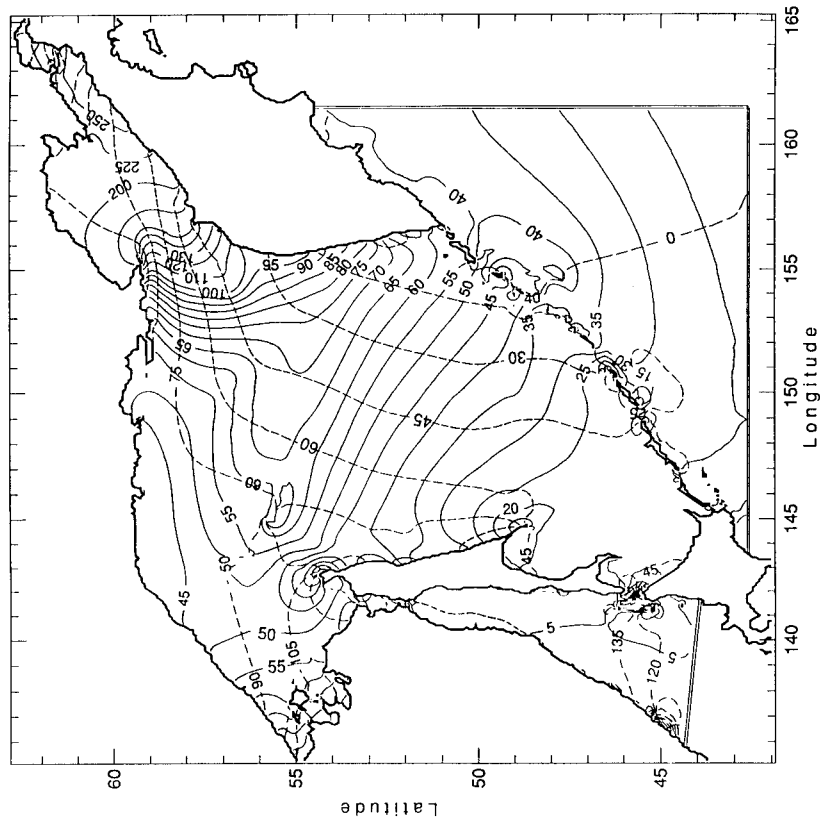


FIG. 2. Computed amplitudes (solid lines, cm) and phases (dashed lines, deg) of surface elevation for the diurnal  $K_1$  tide. The phases are referred to Greenwich; the phase contours are plotted every  $15^\circ$ .

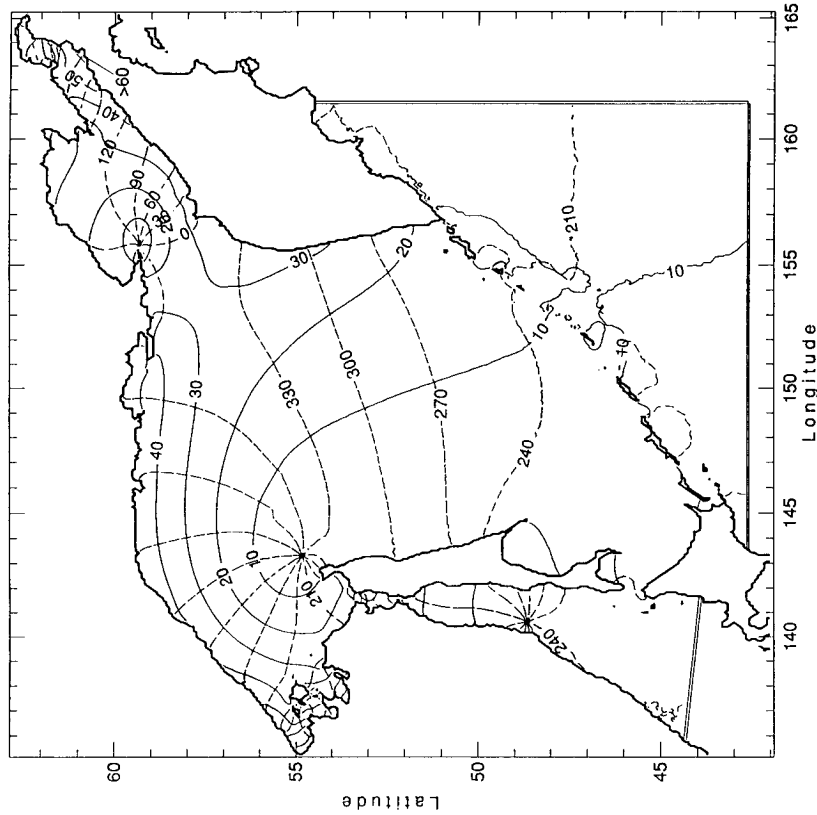


FIG. 5. Computed amplitudes (solid lines, cm) and phases (dashed lines, deg) of surface elevation for the diurnal  $S_2$  tide. The phases are referred to Greenwich; the phase contours are plotted every  $30^\circ$ .

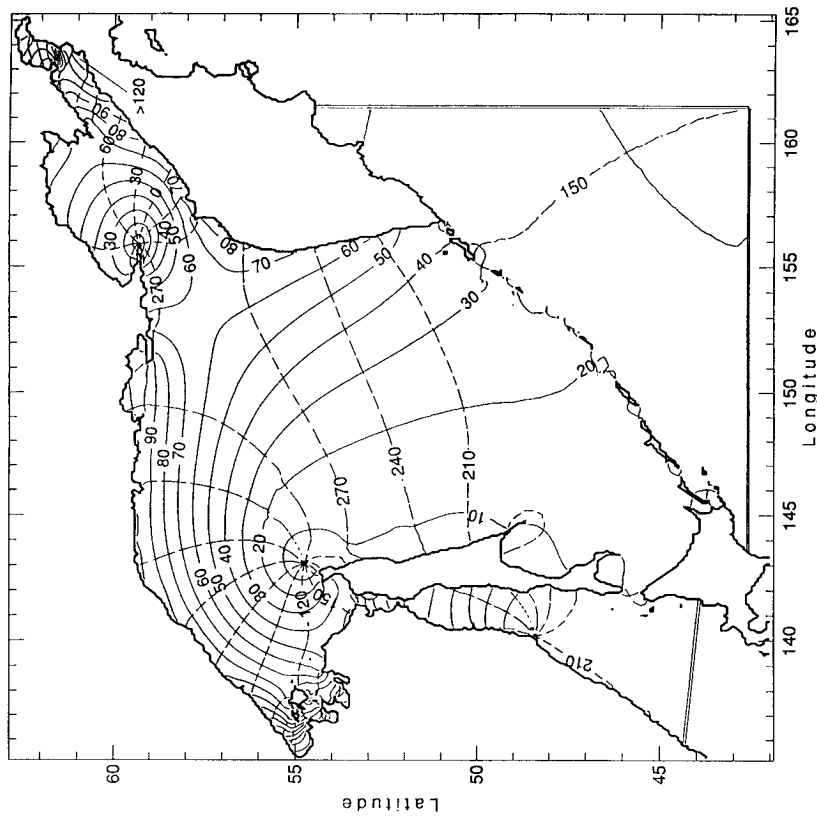


FIG. 4. Computed amplitudes (solid lines, cm) and phases (dashed lines, deg) of surface elevation for the diurnal  $M_2$  tide. The phases are referred to Greenwich; the phase contours are plotted every  $30^\circ$ .

TABLE 1. Comparison of observed and computed tidal amplitudes of the Sea of Okhotsk. In the table NN is the number of stations used in the analysis; Mean and SD are the mean value and standard deviation of the computed and observed time series; Corr and SD1 are the correlation coefficient and standard deviation between the computed and observed data.

Tidal constituent	Amplitude							Phase					
	NN	Mean (cm)		SD (cm)		Corr	SD1 (cm)	Mean (deg)		SD (deg)		Corr	SD1 (deg)
		Com	Obs	Com	Obs			Com	Obs	Com	Obs		
$K_1$	108	32.9	27.8	34.3	32.8	0.965	6.7	111	127	109	113	0.923	18
$O_1$	108	21.6	22.1	17.2	19.8	0.937	6.9	191	182	146	132	0.942	20
$P_1$	21	18.1	15.8	22.3	21.9	0.942	4.0	123	132	72	82	0.776	33
$Q_1$	19	7.5	7.4	6.5	8.2	0.920	5.6	148	148	130	104	0.811	21
$M_2$	108	26.9	29.7	26.3	29.2	0.890	6.3	181	205	69	90	0.869	26
$S_2$	107	12.0	11.0	8.2	9.5	0.824	4.7	213	240	74	90	0.874	26
$N_2$	19	8.6	10.9	5.6	10.8	0.727	4.4	192	207	101	97	0.842	17
$K_2$	21	5.3	5.0	3.7	4.4	0.806	2.1	202	218	99	115	0.887	41

Kuril Islands, Sakhalin, and Hokkaido. At the majority of Russian tidal stations information is available only on  $K_1$ ,  $O_1$ ,  $M_2$ , and  $S_2$  constituents. The main source of information on the minor tidal constituents are 21 stations along Hokkaido and the Kuril Islands.

Statistical analysis of observed and computed sea level data for the eight constituents is shown in Table 1. It includes the number of stations (NN), mean values (Mean) and standard deviations (SD) of the computed and observed series, correlation coefficients (Corr) between computed (Com) and observed (Obs) amplitudes and phases, and standard deviation (SD1) between computed and observed amplitudes and phases. High cor-

relation coefficients attest to satisfactory agreement between the observed and computed sea level. The representative magnitude of errors between measured and computed data for the major constituents ( $K_1$ ,  $O_1$ , and  $M_2$ ) is approximately 6.5 cm in amplitude and 1.0 h in phase. These errors are not distributed uniformly over the coastal line of SO. Due to presence of only 10 stations along northern and eastern shorelines the comparison is skewed toward the Kuril Islands, Hokkaido, and Sakhalin.

To identify the source of these errors the comparison between computed and observed amplitude and phase for a few locations is given in Table 2. Major sources of errors are shallow Penzhinskaya Guba and Udskeya Guba. Whereas in Penzhinskaya Guba, the computed amplitude of 246.5 cm for the  $K_1$  constituent is close to the observed amplitude of 252.1 cm, for the  $M_2$  amplitude the difference between observation and computation is 27.9 cm. A similar situation occurs in Udskeya Guba. The set of experiments carried out in Penzhinskaya Guba indicates that the major cause of these errors is related to the bathymetry. A 4-m increase of depth in Penzhinskaya Guba resulted in a 25% increase of  $M_2$  amplitude and small change in the  $K_1$  amplitude. The  $K_1$  amplitude is less sensitive to small changes in bathymetry, rather, it is influenced by the large-scale resonance conditions.

Generally, the semidiurnal constituents are the least accurate. The higher frequency and shorter wavelength of the semidiurnal waves are more sensitive to small variations of the bathymetry and coastline. The 5' grid smooths local variations of the shallow water bathymetry and the detailed structure of the coastline and narrow straits.

Comparison of the computed cotidal charts for the dominant constituents of the diurnal ( $K_1$ ; Fig. 2) and semidiurnal ( $M_2$ ; Fig. 4) bands of tidal oscillations shows that at the eastern coast of Sakhalin, Kashevarov Bank, the Kuril Islands, and the southwestern part of Kamchatka, local maxima occur in the  $K_1$  pattern, whereas there is no local amplification of the  $M_2$  tidal amplitudes in the same regions. In Figs. 6 and 7 tidal

TABLE 2. Comparison of computed (Comp) and observed (Obs)  $M_2/K_1$  amplitude  $h$  and phase  $g$  at coastal tide gauges.

Gauge	Latitude (N) Longitude (E)	$h$ (cm)		$g$ (deg)	
		Comp	Obs	Comp	Obs
Kuril Islands	44°43'	28.4	28.0	169.3	187.2
	147°21'	32.0	33.0	7.5	7.0
	48°08'	22.0	18.0	169.2	185.3
	153°16'	30.8	29.0	9.1	12.1
	50°50'	39.8	34.0	198.2	229.6
Sakhalin Island	155°39'	59.4	53.0	5.0	352.7
	47°14'	18.8	17.0	186.6	185.8
	143°02'	21.3	19.0	49.0	45.3
	49°14'	29.3	25.0	182.5	182.6
Kamchatka	143°08'	20.2	17.0	42.4	42.2
	50°49'	28.1	22.0	161.1	191.9
	156°30'	47.0	45.0	347.1	354.9
	55°19'	71.4	88.0	253.5	305.0
Penzhinskaya Guba	155°33'	98.9	94.0	26.1	65.0
	62°23'	105.0	132.9	274.6	339.8
	164°30'	246.5	252.1	202.6	183.0
Shelikhov Bay	59°13'	21.6	26.5	237.1	222.5
	155°09'	119.7	123.4	113.9	101.3
Northwestern coast	56°27'	96.2	86.6	85.2	109.6
	138°09'	56.0	45.1	83.9	65.2
Udskeya Guba	54°54'	149.4	181.4	204.3	198.3
	136°46'	68.3	61.0	131.2	96.6

current ellipses for the  $K_1$  and  $M_2$  constituents are shown. General patterns for the other calculated constituents of the diurnal and semidiurnal bands are close to the  $K_1$  and  $M_2$  waves, respectively. Both diurnal and semidiurnal currents increase in shallow areas and straits. Udkaya Guba, Penzhinskaya Guba, Kuril, and Soya Straits are areas of  $M_2$  and  $K_1$  current enhancement. Amplification of the diurnal currents is not, however, limited to these regions. Additional regions occur in proximity to the Kuril Islands, Sakhalin Island, off Hokkaido, over Kashevarov Bank, over escarpments located between Kashevarov Bank and Kamchatka (Fig. 1), and in proximity to Kamchatka. Diurnal band amplification is different from semidiurnal band amplification. The manner in which the amplification takes place over Kashevarov Bank sheds some light on the different physics in these bands. While  $M_2$  currents close to the bank are  $10 \text{ cm s}^{-1}$ , over a tiny portion of the bank the topographic amplification increases currents to  $20 \text{ cm s}^{-1}$ , thus doubling them. The  $K_1$  constituent generates enhanced currents over the whole domain of the bank, amplifying currents approximately 10 times, from  $5\text{--}10 \text{ cm s}^{-1}$  to  $85 \text{ cm s}^{-1}$ . Thus, the different amplification implies that different mechanisms are at work in diurnal and semidiurnal bands of oscillations. In comparing  $M_2$  and  $K_1$  currents near the Kuril Islands, one also notes much stronger enhancement of the diurnal currents.

The energy flux for the  $K_1$  constituent, calculated accordingly to Kowalik and Proshutinsky (1993), is depicted in Fig. 8. The flux of tidal energy is directed from the open boundary in the Pacific through the Kuril Straits toward the region of high frictional dissipation in Shelikhov Bay and Penzhinskaya Guba (big arrows show energy fluxes crossing several transects including open boundaries). The general pattern of energy flow is broken by larger and smaller domains of a circular or semicircular flux of energy. These are regions of trapped tidal energy and enhanced flux. The areas around the Kuril Islands (especially on the Pacific side), Kashevarov Bank, and the entrance to Shelikhov Bay are major domains of trapped energy. Lesser domains are located at escarpments between Kashevarov Bank and the entrance to Shelikhov Bay, along Kamchatka and Sakhalin. The energy flux of the  $M_2$  constituent is given in Fig. 9. The magnitude of the energy flux directed into Shelikhov Bay and Penzhinskaya Guba and into the northwestern region of the SO is similar; therefore, these domains play approximately the same role in dissipation of the  $M_2$  tide. It is difficult to discern the local domains of the circular or semicircular trapping of energy in the energy flux pattern; therefore, one can conclude that semidiurnal waves do not behave like diurnal waves.

Figures 10 and 11 depict the rate of energy dissipation per unit surface in the SO due to  $K_1$  and  $M_2$  constituents, respectively. Again, these figures demonstrate the difference in the dissipation pattern of diurnal and semidiurnal tides in the SO. The trapping of the energy flux

over local bathymetry depicted in Fig. 8 for the  $K_1$  constituent resulted in the local maxima for the rate of energy dissipation (Fig. 10). Patterns of dissipated energy in Figs. 10 and 11 are in close agreement with computations made by Suzuki and Kanari (1986). The balance of tidal energy is presented in Table 3. Terms in the energy conservation equation were calculated according to Marchuk and Kagan (1989). The total flux of energy across open boundaries and the overall rate of energy generation due to astronomical tidal forcing is balanced by the total rate of energy dissipation. The net energy flux through the open boundaries is the principal source of energy. The overall rate of energy generated by astronomical forces is relatively small. For the  $K_1$  tide astronomical forces generate only 6% of the total energy. Slight discrepancies between the sources and sinks of energy in Table 3 are due to errors associated with the averaging of the velocity components in the staggered C-grid used in the computations.

The total rate of energy dissipation due to  $M_2$  tide, averaged over one tidal period, is estimated to be  $49.2 \times 10^{16} \text{ erg s}^{-1}$  in the entire SO. This magnitude is close to  $40.0 \times 10^{16} \text{ erg s}^{-1}$  given by Jeffreys (1920), but is smaller than  $73.0 \times 10^{16} \text{ erg s}^{-1}$  derived by Lyard and LeProvost (1997) and is much smaller than  $210.0 \times 10^{16} \text{ erg s}^{-1}$  estimated by Miller (1966). We did not find any reference to the overall rate of energy dissipated in the diurnal band of oscillation for comparison against data given in Table 3. According to our results, more than 60% of the  $K_1$  energy is dissipated in Shelikhov Bay and Penzhinskaya Guba (Fig. 9); therefore, this rather small basin has a very important role in the balance of tidal energy.

Due to variable bathymetry, strong oscillating diurnal and semidiurnal currents transfer vorticity to the mean motion, generating residual currents through the nonlinear interaction. In Fig. 12 residual currents due to the eight major constituents are depicted. The maximum velocity is close to  $16 \text{ cm s}^{-1}$  in a numerical lattice of approximately 6.5-km resolution. To extract residual motion, tidal currents were averaged over a 29-day period. The residual circulation shows well-developed trapped eddies over Kashevarov Bank, in proximity to Kuril Islands and in the Shelikhov Bay–Penzhinskaya Guba area. Stationary clockwise eddies in the proximity of the Kuril Islands were described by Yefimov et al. (1985), but only recently Rogachev et al. (1996) demonstrated, with the help of Argos buoys and in situ measurements, that the diurnal tide is the source of energy for these eddies.

To investigate behavior of the numerical model in the shelf wave regions we first compare the model to measurements off the coast of Hokkaido. This region is well described through observations of tidal amplitude and current made by Aota and Matsuyama (1987) and Odamaki (1994). Odamaki carried out current meter observations in many locations at the 10-m level for one summer month, while Aota and Matsuyama measured

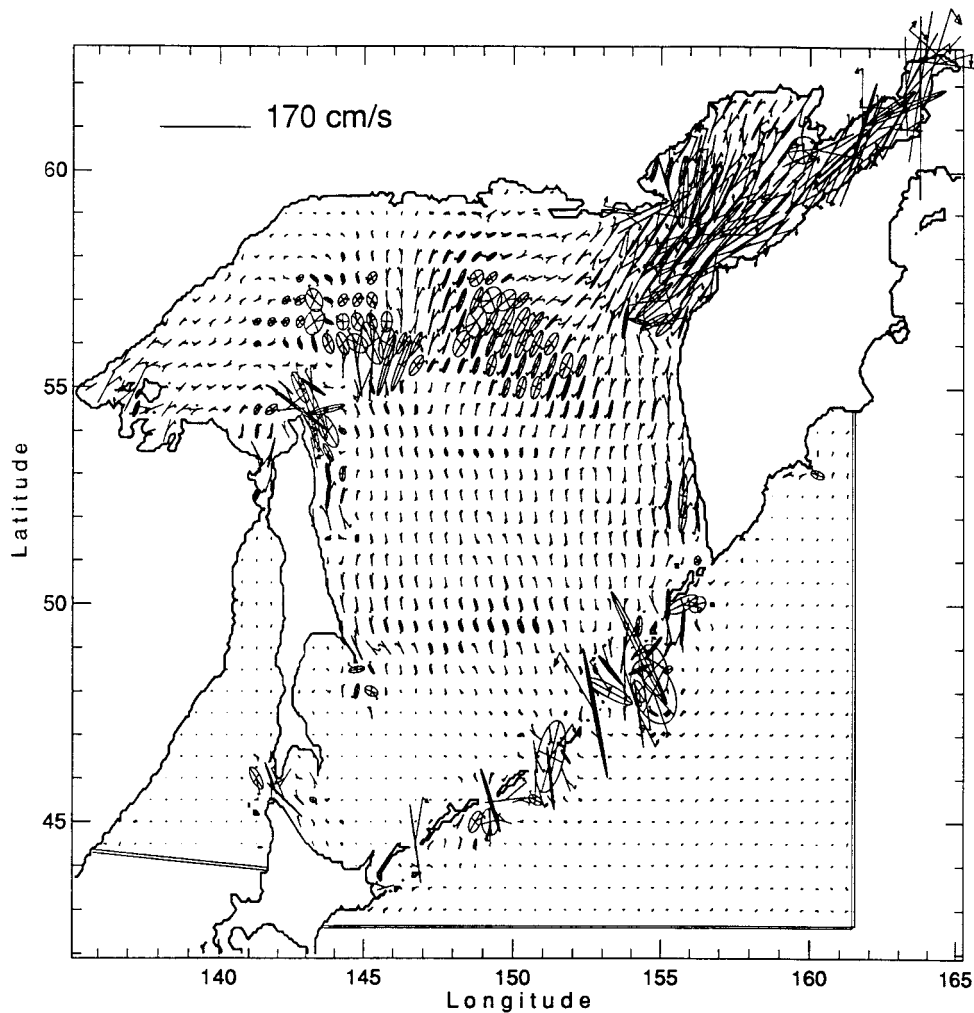


FIG. 6. Computed  $K_1$  tidal current ellipses. Ellipses are depicted at every sixth point of numerical grid. The arrow at each ellipse shows the direction of rotation.

current from February 1980 to September 1982 at a single location. This current meter was deployed at the 20-m level in a water depth of 35 m. The long time record was divided into 150-day segments by Aota and Matsuyama to study time variability of the currents. Observed and calculated sea level amplitudes and phases for major tidal constituents are given in Table 4. The calculated elevations are in close agreement with those obtained from observations.

Table 5 contains calculated and observed harmonic constants for the tidal currents (orientation of the major axis is relative to the north). This table shows that the model produced realistic diurnal tidal currents along the straight part of the coast [from station 1 to station 9 in the Aota and Matsuyama (1987) notation]. The calculated and observed diurnal tidal velocities are in agreement at Soya Strait northern station S1, whereas at the southern station S2 the observed current is almost twice as large as the calculated current. The reason for this underestimation seems to be proximity to the nodal

point in Soya Strait where a small change in the nodal point location may cause a large change in current. The strong spatial variability of diurnal currents in the vicinity of the nodal point is corroborated by Odamaki (1994). According to his measurements the major axis of the tidal ellipse at two stations in Soya Strait differs by  $29 \text{ cm s}^{-1}$ . Observed tidal current amplitudes have noticeable time variability. The nature of this variability remains uncertain (Aota and Matsuyama 1987). Because density stratification is weak and tidal temperature fluctuations do not occur in the observed temperature records, the internal tides must be rejected as a source of this variability. Due to low phase velocity of the shelf wave the occurrence of variability in the diurnal band may be related to the interaction of the Soya Current with the shelf wave. Some variability may be caused by the nonlinear interaction of the various tidal constituents. As demonstrated in Table 5, the length of the major axis of the  $K_1$  tidal current ellipses varied in time from 19.6 to  $33.5 \text{ cm s}^{-1}$  at station 2 in 1980–82 (Aota

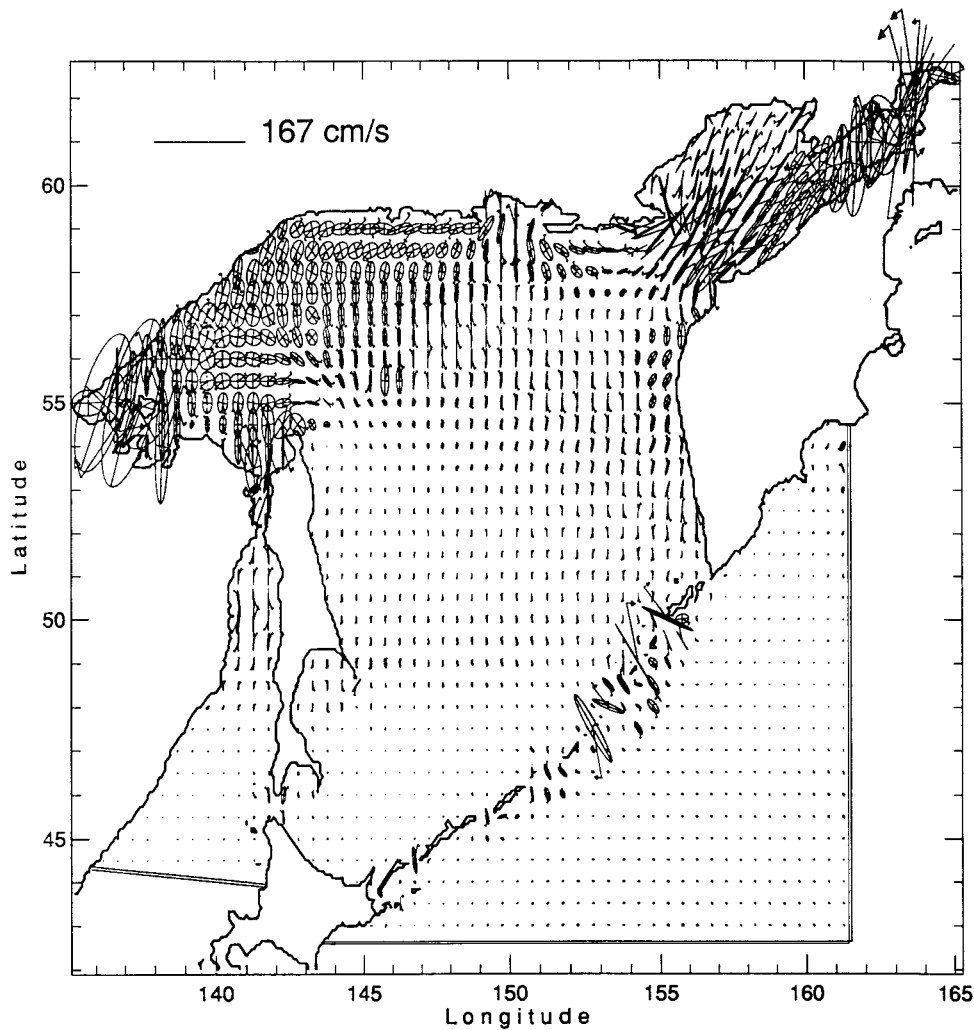


FIG. 7. Computed  $M_2$  tidal current ellipses. Ellipses are depicted at every sixth point of numerical grid. The arrow at each ellipse shows the direction of rotation.

and Matsuyama 1987). The phase and orientation of the tidal ellipses are very stable. According to Odamaki (1994), the major axis at the same station is only  $12.3 \text{ cm s}^{-1}$ . The computed value falls in this range and equals  $22.5 \text{ cm s}^{-1}$ .

Odamaki (1994) suggested that the difference between the tidal amplitude and phase of the SO and the Sea of Japan generates a shelf wave, which propagates along the coast of Hokkaido from Soya Strait. The observed phase velocity of the  $K_1$  tidal current is equal to  $5.5 \text{ m s}^{-1}$ . This almost coincides with the estimate of the phase velocity of  $6.6 \text{ m s}^{-1}$  for the first mode of the shelf wave obtained by using a simple analytical model (Clarke 1991). Odamaki calculated the travel time (phase lag) of the shelf wave from Soya Strait, for all stations given in Table 5, using a phase speed of  $5.5 \text{ m s}^{-1}$  and distances between the stations and Soya Strait. In Fig. 13 the relation between the phase lags of the  $K_1$  tidal currents and station distances from Soya Strait ac-

cording to Odamaki and to our computation is shown. The computed phase velocity of the  $K_1$  tidal current is  $7.1 \text{ m s}^{-1}$ .

#### 4. Tides over Kashevarov Bank

The selective interaction of diurnal and semidiurnal tides with a seamount is exhibited over Kashevarov Bank. There are no large peculiarities in the cotidal charts of the semidiurnal tides there (Figs. 4 and 5). Increase in the semidiurnal tidal currents is relatively small (Fig. 7) when compared to the diurnal currents (Fig. 6).

A special behavior of the diurnal tides around Kashevarov Bank is easily detected in energy flux and dissipation charts (Figs. 8 and 10). Tidal energy is trapped around the bank and the rate of energy dissipation depicts a local maximum there. A noticeable transformation of the diurnal amplitudes and currents is also

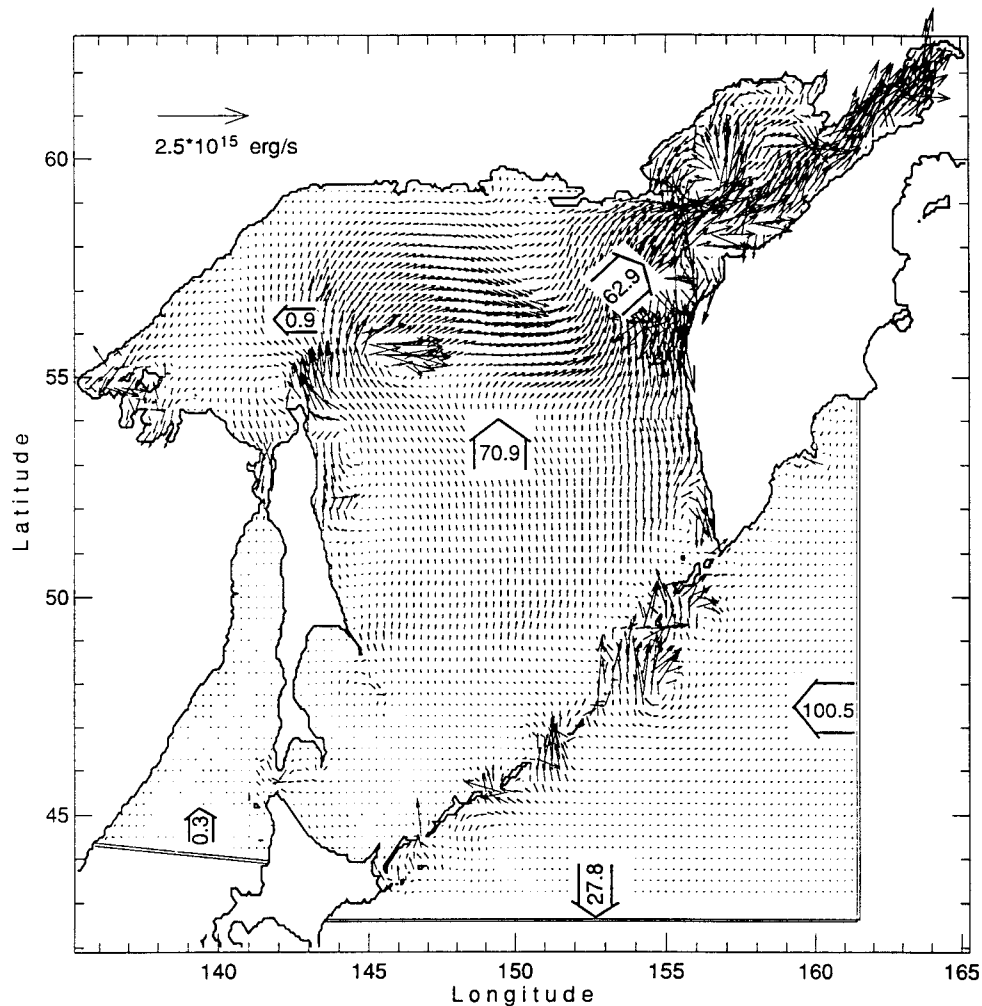


FIG. 8. Tidal energy flux for  $K_1$  wave. Large arrows show the net energy flux through transects. The values inside arrows should be multiplied by  $10^{16}$  erg  $s^{-1}$ .

evident. Results are discussed for the dominant  $K_1$  constituent. The cotidal chart of the  $K_1$  constituent for the Kashevarov Bank region is shown in Fig. 14. The amplitude at the top of bank increases, reaching a maximum of 65 cm. A similar pattern in the  $O_1$  tidal level oscillations occurs as well. The maximum current for  $K_1$  (Fig. 15) and  $O_1$  (not shown) is 85 and 75  $cm\ s^{-1}$ , respectively, relative to off-bank values of 5–10  $cm\ s^{-1}$ . The circular shape of the tidal current ellipses above the bank (Fig. 6) changes to rectilinear oscillations at the steepest slopes of the bank, located south and southwest from the top of the bank. This tidal flow behavior is typical for trapping or partial trapping of tidal energy by bottom irregularity (Kowalik 1994).

Local behavior of tidal oscillations often depends on the resonance phenomena in local water bodies (e.g., Platzman 1972). To demonstrate the possibility of resonance we depict the distribution of natural oscillations in the SO and especially at Kashevarov Bank over the range of diurnal and semidiurnal tides. The investigation

is done with the help of the basic set of equations (1)–(3), but the nonlinear and frictional effects are neglected. Sea level is set to zero at the open boundaries and at the solid boundaries the normal derivative of velocity vanishes. To force oscillation through this system of equations one can apply initial forcing at the open boundary or over the entire domain (Marchuk and Kagan 1989). We utilize the latter approach and a random sea level distribution is prescribed initially. With such initial and boundary conditions the set of equations (1)–(3), without nonlinear and frictional terms, is integrated in time. Because this set of equations is conservative, the system is allowed to oscillate for a long enough time so that the initial oscillations are redistributed to various portions of the free wave spectra. After an initial period of 100 h the stationary regime occurs and the model is run for 1024 h. The series of hourly data is used for the power spectra analysis of amplitude and velocity of oscillations over the whole SO. The natural period of 26.3 h occurs in the entire SO both in the sea level and in

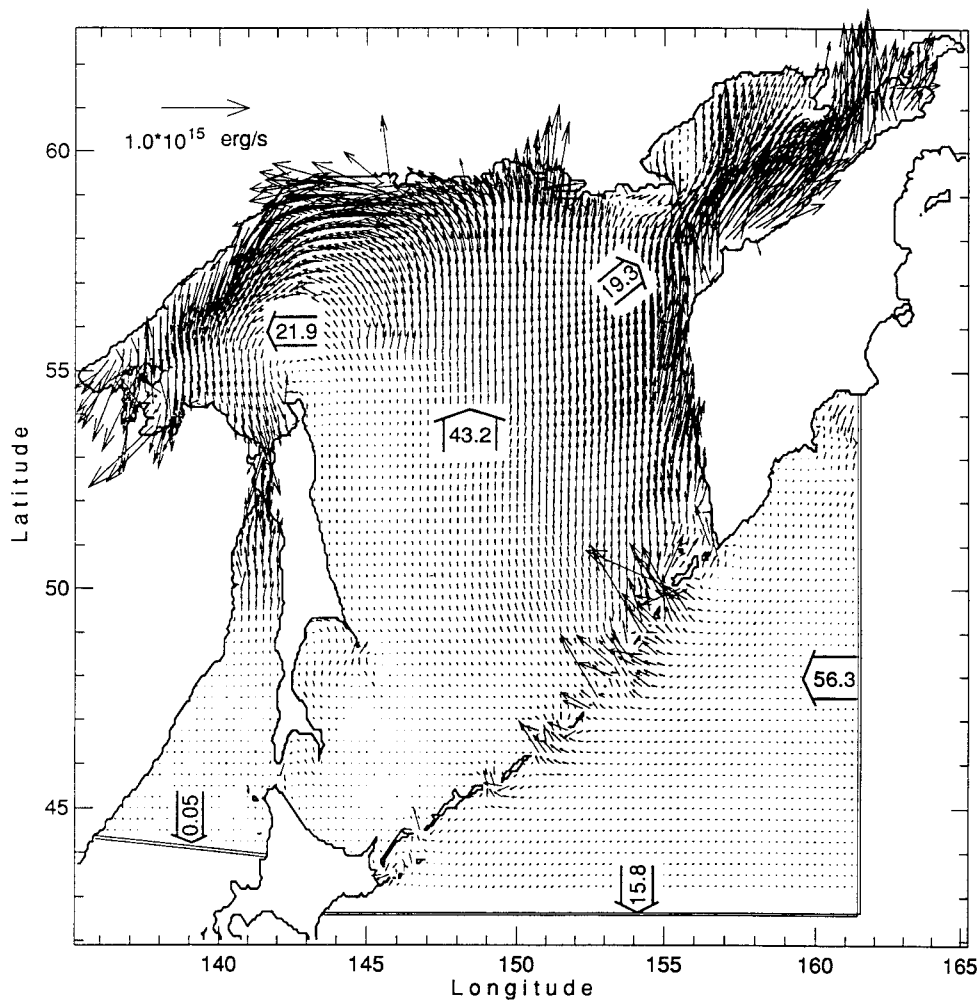


FIG. 9. Tidal energy flux for  $M_2$  wave. Large arrows show the net energy flux through transects. The values inside arrows should be multiplied by  $10^{16}$  erg  $s^{-1}$ .

velocity spectra. This period is very close to the  $O_1$  period (25.82 h), therefore enhancement of the  $O_1$  tide occurs, but the 26.3 h resonant peak is broad and some enhancement of oscillations takes place at the  $K_1$  period (23.93) as well. Observations taken near Sakhalin Island (Rabinovich and Zhukov 1984), off Hokkaido (Odamaki 1994), and at the Kuril Islands (Yefimov et al. 1985) show that the  $O_1$  constituent is much more amplified than the  $K_1$  constituent, corroborating the possibility of resonance enhancement in the entire SO through a 26.3-h oscillation.

At the given spectral band, as Marchuk and Kagan (1989) showed, the enhancement of oscillations of sea level and velocity caused by resonance can be investigated through the spatial distribution of sea level and velocity of the free oscillations over the same spectral band. For the SO, the velocity and sea level of the free oscillations obtained above are filtered using the technique described by Marchuk and Kagan. After filtration, the velocity at the given period is weighted by its stan-

dard deviation taken over the entire SO. Therefore, the spatial distribution of the normalized velocity represents coefficient of amplification. A similar technique is applied to the sea level amplitude. This approach gives a possibility for comparison of enhancement over the various domains of the SO. For example, the largest amplification of the elevation amplitude of diurnal constituents occurs in Shelikhov Bay and Penzhinskaya Guba. The amplification coefficient for the diurnal tide over these regions is approximately 10 times greater than over Kashevarov Bank.

In Fig. 16 spatial distributions of the amplification coefficient for the sea level (left side of Fig. 16) and for the maximum velocity (right side of Fig. 16) are given over Kashevarov Bank at three periods in the diurnal range of oscillations: the natural oscillation period of 26.3 h (top), the  $O_1$  constituent (center), and the  $K_1$  constituent (bottom). The spatial location of the sea level and velocity maxima differs for the different periods, and for the  $K_1$  and  $O_1$  periods compares well with

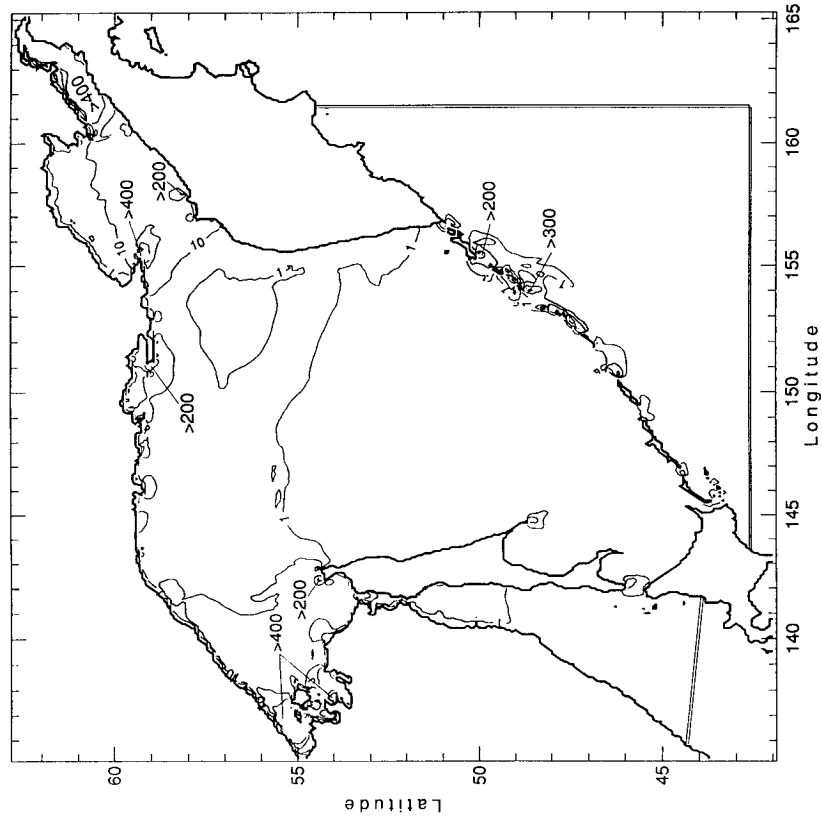


FIG. 11. The rate of energy dissipation per unit surface due to the  $M_2$  constituent ( $\text{erg s}^{-1} \text{cm}^{-2}$ ).

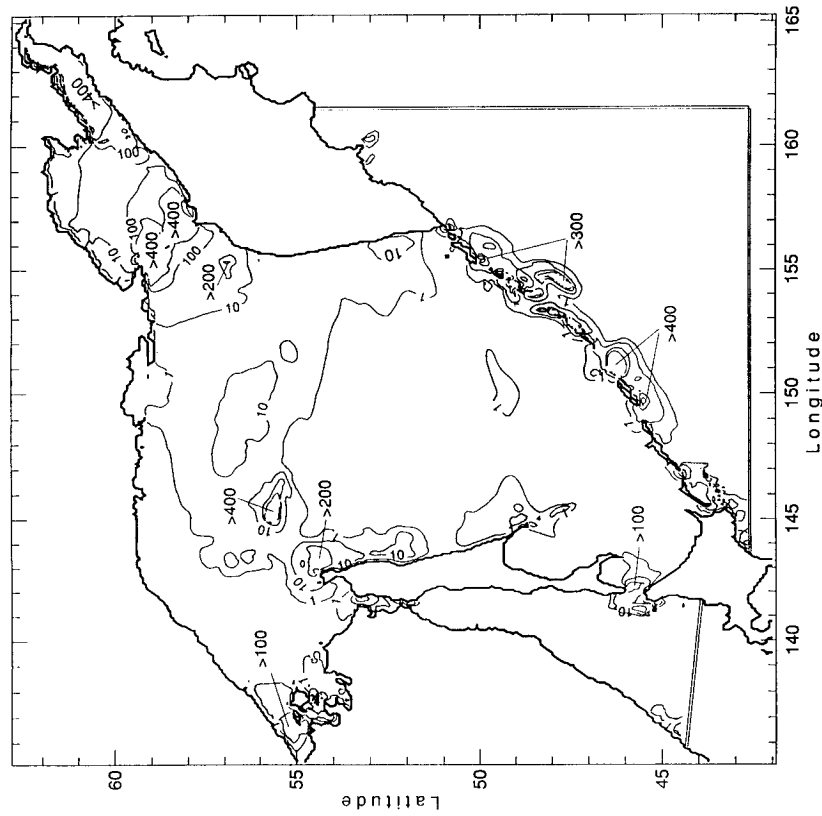


FIG. 10. The rate of energy dissipation per unit surface due to the  $K_1$  constituent ( $\text{erg s}^{-1} \text{cm}^{-2}$ ).

TABLE 3. Energy balance for the major tidal constituents.

	Source ( $\times 10^{16}$ erg $s^{-1}$ )					Sink ( $\times 10^{16}$ erg $s^{-1}$ )			
	$K_1$	$O_1$	$M_2$	$S_2$		$K_1$	$O_1$	$M_2$	$S_2$
Net energy flux through open boundary:					Overall rate of energy dissipation due to:				
Japan Sea	0.3	0.3	-0.05	0.00	bottom friction	58.1	17.5	39.9	3.4
southern boundary	-27.8	-11.4	-15.8	-1.3	horizontal friction	20.2	7.8	9.3	1.1
eastern boundary	100.5	34.4	56.3	5.4					
Overall rate of energy generation due to astronomical forcing	4.7	1.3	8.1	0.5					
Total	77.7	24.6	48.6	4.6		78.2	25.2	49.2	4.5

the location of the computed maxima for the tides (see Figs. 14 and 15). In Fig. 16 the coefficient of amplification for the amplitude decreases for the shorter periods, whereas in some locations the amplification of current is stronger at the  $K_1$  period than at the  $O_1$  period. It follows from the above results that the resonant enhancement of velocity and sea level at the  $O_1$  period is caused by proximity of the natural oscillation period

and  $O_1$  period. The strong amplification coefficient of velocity at the  $K_1$  period shows that the resonant amplification of velocity is substantial for a wide range of periods.

The nonlinear interaction of tidal constituents above a seamount is an important element of tidal dynamics. Recent studies, based on current observations over Fieberling Guyot in the North Pacific (Brink 1995) and on

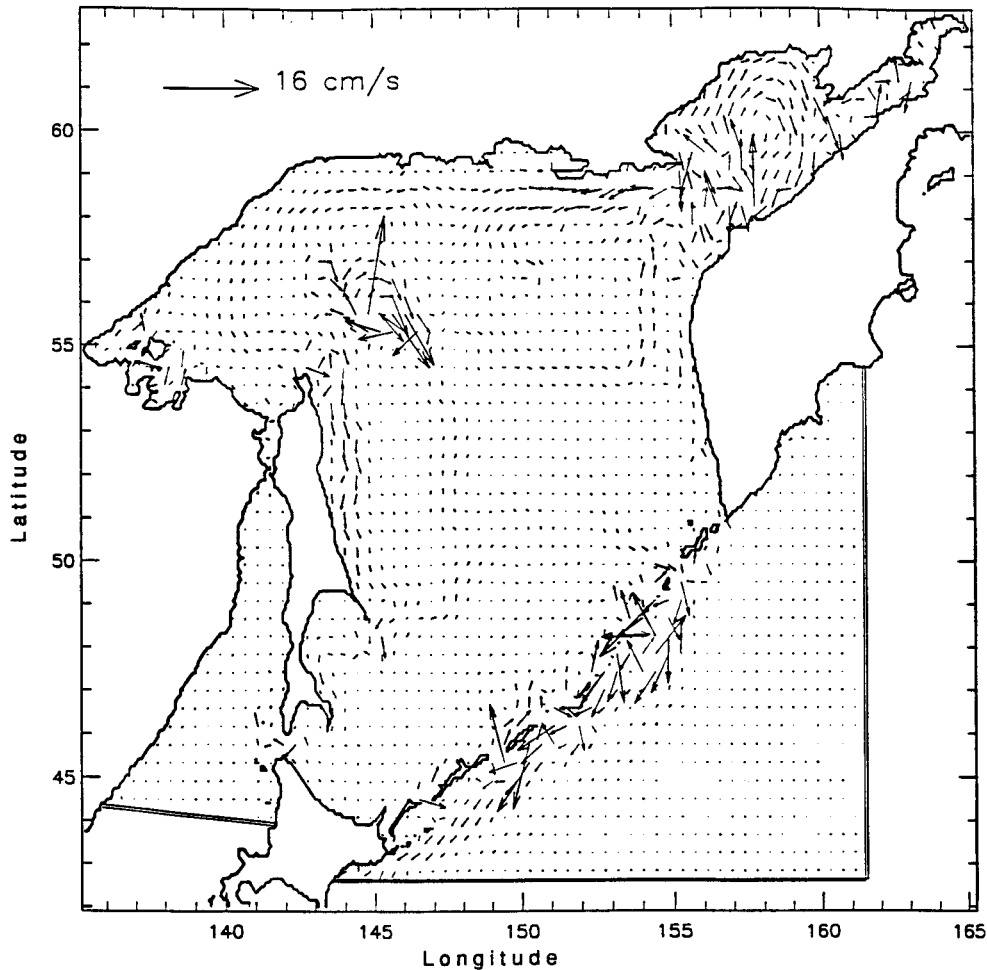


FIG. 12. Residual tidal currents due to eight tidal constituents. Vectors are shown at every fifth grid point.

TABLE 4. Comparison of observed (upper row) and computed (lower row) tidal amplitudes ( $A$ ) and phases (Ph) along Hokkaido Island.

Station	Lat (N)	Long (E)	$K_1$		$O_1$		$M_2$		$S_2$	
			$A$ (cm)	Ph (deg)	$A$ (cm)	Ph (deg)	$A$ (cm)	Ph (deg)	$A$ (cm)	Ph (deg)
1	45°25'	141°41'	7	238	7	215	3	199	2	233
			4.0	226	4.1	216	1.4	193	3.8	250
2	45°31'	141°57'	5	356	4	344	6	193	4	247
			6.0	25	3.5	8	11.5	191	6.0	249
3	44°56'	142°36'	17	38	17	17	17	174	8	221
			19.9	35	16.0	22	24.6	194	8.1	238
4	44°35'	142°58'	20	42	20	18	17	178	8	221
			21.5	42	18.6	29	25.5	196	8.3	239
5	44°21'	143°22'	22	48	23	24	18	176	8	218
			21.8	45	19.4	33	25.5	197	8.3	240
6	44°01'	144°16'	21	72	21	35	18	186	8	240
			21.1	48	18.1	39	24.3	199	8.1	241
7	43°44'	145°27'	27	27	22	350	29	169	13	223
			25.7	20	17.1	37	31.2	201	12.5	244
8	44°02'	145°51'	27	11	18	322	30	152	13	205
			21.2	10	16.7	6	38.5	196	13.0	222
9	43°20'	145°35'	23	28	18	350	31	166	14	219
			25.8	21	16.7	20	31.5	184	16.5	235

investigations by Butman et al. (1983), show that the nonlinear interaction of diurnal constituents  $K_1$  and  $O_1$  results in new oscillations with periods at the semidiurnal  $M_2$  tidal frequency (sum of  $K_1$  and  $O_1$  frequencies) and a fortnightly tide (difference of  $K_1$  and  $O_1$  frequencies) with a 13.66-day period. The rectification of the strong diurnal currents produces a mean (residual) clockwise circulation around the seamount.

We applied this mechanism to study nonlinear tidal interaction over Kashevarov Bank due to the two major constituents  $K_1$  and  $O_1$ . A series of experiments was carried out to assess the effects of nonlinear interactions of these constituents and to demonstrate the balance between a linear and nonlinear tendency in the tidal velocity.

The sum of  $K_1$  and  $O_1$  tides in the SO was calculated by the same equations as those used for the eight tidal waves computation. The boundary conditions at the open boundaries and astronomic forcing included only the  $K_1$  and  $O_1$  sea level oscillations. The energy of the system became stationary after one month, but we continued the calculation to obtain a three-month time series. Two sets of experiments were carried out: 1) all nonlinear terms are included and 2) nonlinear advective terms are rejected and bottom friction terms are linearized. Comparison of results with and without advective terms and nonlinear bottom friction in the equations of motion shows that their omission removes the residual circulation. To investigate the differences between linear and nonlinear tidal dynamics, we considered the temporal variability of the tidal currents. The time series of the tidal currents at point P (see Fig. 14) over Kashevarov Bank after 30 days of simulation is shown in Fig. 17 for both nonlinear and linear cases.

The temporal variability of the tidal currents resulting from the interaction of  $K_1$  and  $O_1$  constituents exhibits

a fortnightly (13.66 day) oscillation that constitutes the upper and lower envelope of the diurnal signals (Fig. 17). In the linear case (Fig. 17, top) the fortnightly envelopes of the positive and negative values are symmetrical and no residual currents are generated. In the nonlinear case the upper and lower envelopes of the tidal currents are asymmetrical (Fig. 17, bottom). The values of the upper envelope of the north–south ( $V$ ) velocity component are greater than those of the lower envelope, resulting in a 13–14 cm s<sup>-1</sup> residual current. Particularly striking is the difference of 45 cm s<sup>-1</sup> between the upper and lower envelopes of the east–west ( $U$ ) velocity component.

For additional analysis we used a digital filter tuned to the narrow frequency band around  $K_1$  and  $O_1$  constituents. The digital filter was constructed by IDL and it allows us to apply a variable number of the filter weights (IDL Reference Guide 1995, 1–235). To achieve proper resolution we used a three-month time series of hourly values and a filter with 501 weights. This filter loses 501 h (close to 21 days) from each end of the original time series. Some results of filtration for the east–west component at point P over Kashevarov Bank for the fully nonlinear solution are given in Fig. 18. The top portion depicts results of filtration at the  $K_1$  period and the bottom shows a 13.66-day period and mean residual current derived by low-pass filter. The  $K_1$  tidal current over Kashevarov Bank is modulated by a fortnightly period. The energy alternates between the  $K_1$  period and fortnightly period when the  $K_1$  constituent oscillates with the maximum velocity the minimum of the fortnightly velocity occurs and vice versa. The fortnightly modulation is different at various points of the domain due to different intensity of the fortnightly currents. In Fig. 19 the fortnightly current ellipses are shown. The maximum fortnightly current is close to 7

TABLE 5. Comparison of observed (upper row) and computed (lower row) tidal current ellipses along Hokkaido Island:  $L$  is the length of the major axis and  $S$  is the length of the minor axis of the tidal ellipse ( $\text{cm s}^{-1}$ ),  $\text{Dir}$  is orientation of the major axis (deg). The upper row is from observations (Odamaki 1994); the lower row is from modeling. Observations by Aota and Matsuyama (1987) are denoted as 2a–2e.

Station	Latitude	Longitude	$K_1$			$O_1$			$M_2$			$S_2$		
			$L$	$S$	Dir	$L$	$S$	Dir	$L$	$S$	Dir	$L$	$S$	Dir
S1	45°48'	142°03'	62.2	14.9	138	80.2	11.3	130	27.3	16.5	165	10.3	6.7	160
			60.4	4.6	114	46.6	4.5	112	26.2	3.0	80	8.9	0.6	77
S2	45°38'	141°59'	91.6	2.6	143	98.3	10.8	141	35.5	23.7	174	15.4	10.3	228
			47.6	4.7	114	51.1	3.3	84	19.6	0.6	105	12.2	0.8	100
1	45°28'	142°27'	21.1	6.7	135	21.1	3.1	131	5.7	3.6	99	5.1	1.5	82
			17.4	1.7	117	18.9	1.4	120	5.3	0.0	103	1.9	0.1	104
2	45°18'	142°19'	12.3	0.5	137	11.3	0.5	140	3.6	0.5	135	2.1	0.5	130
			29.7	4.7	152	29.4	3.5	141	9.7	0.8	145	3.3	0.5	146
			19.6	1.7	142	25.4	1.9	148	8.8	0.5	144	2.9	0.2	134
			27.9	1.9	160	21.9	1.9	154	8.5	1.1	147	2.5	0.8	149
			33.5	5.3	153	35.2	3.7	150	10.9	0.8	141	5.1	0.8	148
			30.6	5.1	151	37.7	3.5	152	14.1	1.1	144	4.6	1.3	145
3	45°11'	142°40'	22.5	1.2	135	17.4	3.8	107	6.7	0.4	129	2.5	0.0	126
			11.3	3.6	131	10.8	5.1	107	3.6	1.0	22	4.1	1.5	203
4	45°11'	142°30'	9.9	0.6	136	9.8	1.2	121	1.9	0.1	146	0.6	0.0	168
			16.5	5.1	144	15.9	3.1	154	3.6	1.0	231	3.1	0.5	75
5	44°56'	142°56'	13.1	0.5	140	11.4	0.9	120	2.8	0.1	143	0.9	0.1	157
			8.2	0.5	141	6.7	0.5	142	2.1	0.0	144	3.6	1.5	163
6	44°15'	142°44'	7.3	0.5	140	8.7	1.0	136	1.2	0.0	194	0.4	0.2	187
			8.7	0.0	146	7.2	0.0	147	1.0	0.5	158	1.0	0.5	118
7	44°41'	143°12'	8.0	0.2	147	8.1	0.5	137	1.2	0.1	191	0.4	0.0	191
			6.2	0.0	127	7.2	3.1	166	1.5	0.5	74	3.6	1.5	19
8	44°36'	143°05'	4.7	0.3	139	6.7	0.3	135	1.1	0.0	225	0.4	0.1	187
			7.2	1.0	140	6.7	0.5	135	0.5	0.5	173	0.5	0.0	15
9	44°34'	143°34'	4.8	0.0	143	6.9	0.3	135	0.9	0.1	228	0.3	0.0	219
			5.1	0.5	133	8.7	0.5	133	1.5	0.0	159	3.1	1.0	55
			3.8	0.6	132	6.5	0.9	131	1.4	0.1	237	0.5	0.1	236

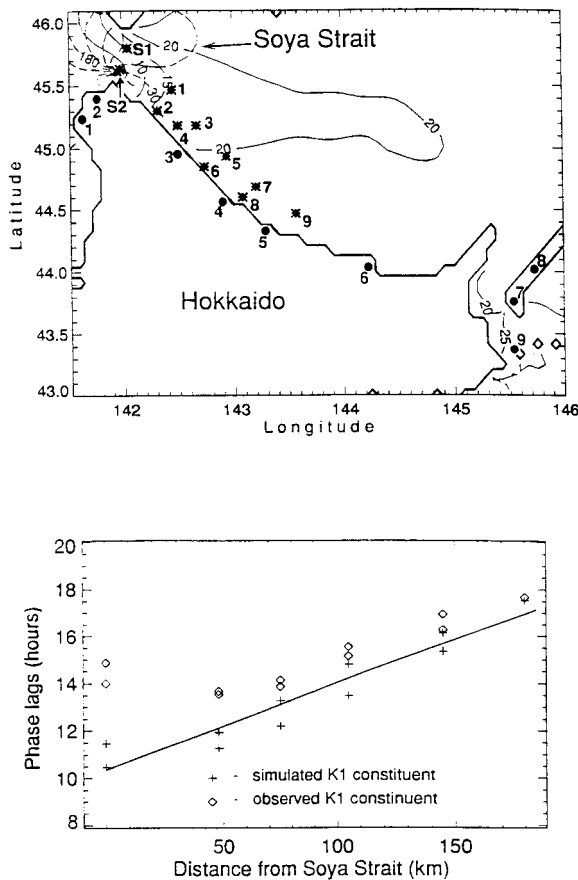


FIG. 13. (top) Computed amplitudes (solid lines, cm) and phases (dashed lines, degrees) of surface elevation for the  $K_1$  tide at the northern coast of Hokkaido. Stars and numbers show the location and numbering of current stations taken by Aota and Matsuyama (1987). Dots and numbers show the location and numbering of the coastal sea level gauges. (bottom) Phase lags (travel time) from Soya Strait to measuring stations. The diamonds denote Odamaki's (1994) observations, crosses are results of computations, and the solid line shows a least squares fit to computations.

$\text{cm s}^{-1}$ . The distribution of tidal ellipses depicts opposite rotation of the tidal currents at the northern and southern slopes of Kashevarov Bank.

To investigate further the nonlinear interaction of the two diurnal constituents on tide formation, we describe a few additional properties. The fortnightly oscillations represent a rather strong variation in velocity. However, this variation is not reflected as strongly in the sea level oscillations because the maximum fortnightly sea level change is 10 cm. The nonlinear interaction of the diurnal tides influences the pattern of the  $M_2$  constituent. The  $K_1$  and  $O_1$  tides generate a rather strong current at the  $M_2$  frequency (Fig. 20). The current shows a maximum of approximately  $9 \text{ cm s}^{-1}$  at the top of Kashevarov Bank where the nonlinear interactions are greatest and rapidly diminishes to  $1 \text{ cm s}^{-1}$  off the bank where the nonlinear terms are small. The  $9 \text{ cm s}^{-1}$  current is approximately a half of the total  $M_2$  tidal current above

the bank, as computed by the model which incorporated the eight tidal constituents (Fig. 7). The nonlinear interaction of the diurnal tides has no significant effect on sea level at the  $M_2$  tidal frequency and the maximum of amplitude is approximately 1 cm at the bank top.

To identify additional important aspects of the interaction of  $K_1$  and  $O_1$  constituents, power spectra based on FFT with the Hanning spectral window were employed. The purpose of these experiments was to learn how energy is redistributed from the major tidal constituents,  $K_1$  and  $O_1$ , to various parts of the tidal spectra for the linear and nonlinear interactions. Magnitudes of the energy spectra at  $O_1$  and  $K_1$  periods for the nonlinear and linear experiments are governed by different physics. These magnitudes are controlled by bottom friction, and only nonlinear bottom friction [Eq. (5)] reproduces tidal amplitude well. The linearized formula is based on mean values that do not take local conditions into account.

The power spectra of the east–west component of the tidal current at point P is given in Fig. 21. The linear result is shown in the top panel, the full nonlinear interaction is given in the center panel, and the nonlinear interaction without advective terms (only nonlinear bottom friction remains) in the equation of motion is depicted in the bottom panel.

The power spectrum for the linear problem (Fig. 21, top) shows only one major maximum with energy at  $K_1$  and  $O_1$  wave periods. In the case of nonlinear interaction, the existence of several major and minor maxima in the power spectra (Fig. 21, center) is revealed. The major maxima occur at the semidiurnal, diurnal, and fortnightly periods. Minor maxima are located close to 8 and 6 h. The major maxima can be explained by nonlinear interaction of two original tidal constituents (the so-called compound tides). Moreover, each basic constituent ( $K_1$  or  $O_1$ ) produces, through the nonlinear terms, overtones represented in the power spectra as both major and minor maxima. Assuming the  $K_1$  period to be  $T_{K_1}$ , this constituent through the advective terms, generates overtide oscillations whose periods are  $T_{K_i} = T_{K_1}/2i$  (Parker 1991). Overtones due to nonlinear bottom friction are  $T_{K_i} = T_{K_1}/(2i + 1)$ . Here  $i = 1, 2, 3, \dots$ . Thus, for the  $K_1$  tide, the major overtones are located at 11.96 and 5.98 h (due to advective terms) and 7.98 h (due to bottom friction) and, for the  $O_1$  tide the major overtones are at 12.91 and 6.45 h (due to advective terms) and 8.61 h (due to bottom friction). In the semidiurnal band, the power spectra depict a large maximum of energy caused by several oscillations: a compound tide at the  $M_2$  tide period, an overtide due to the  $K_1$  tide at 11.96 h, and an overtide due to the  $O_1$  tide at 12.91 h. In the bottom plot, the nonlinear interaction is caused by the bottom friction only (i.e., advective terms are neglected), the dominant oscillation is located at the diurnal band, and the first higher harmonic is, as one would expect, close to 8 h. The latter maximum is of secondary magnitude and one can conclude that the bot-

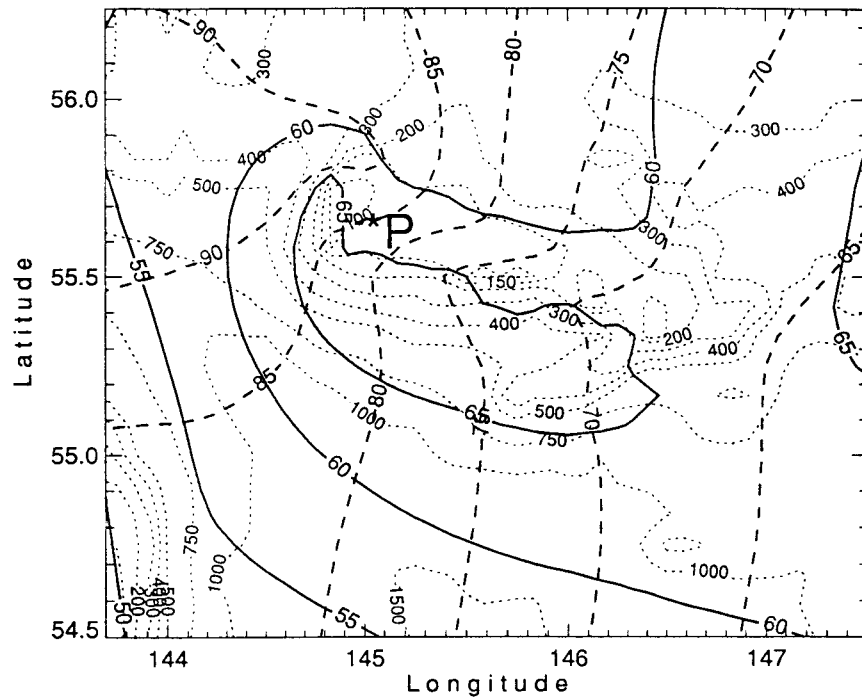


FIG. 14. Computed amplitudes (solid lines, cm) and phases (dashed lines, deg) of surface elevation for the  $K_1$  constituent above Kashevarov Bank. Bathymetry in meters is given by dotted lines. Point P denotes location for the time series analysis.

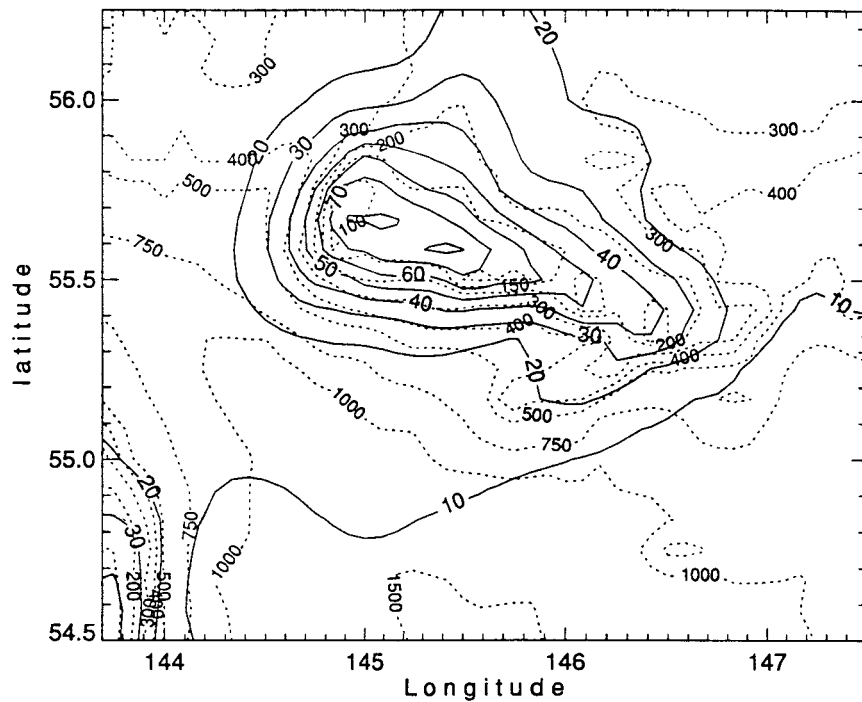


FIG. 15. Contours of the maximum  $K_1$  tidal currents (solid lines,  $\text{cm s}^{-1}$ ) and bathymetry (dotted lines, m) above Kashevarov Bank.

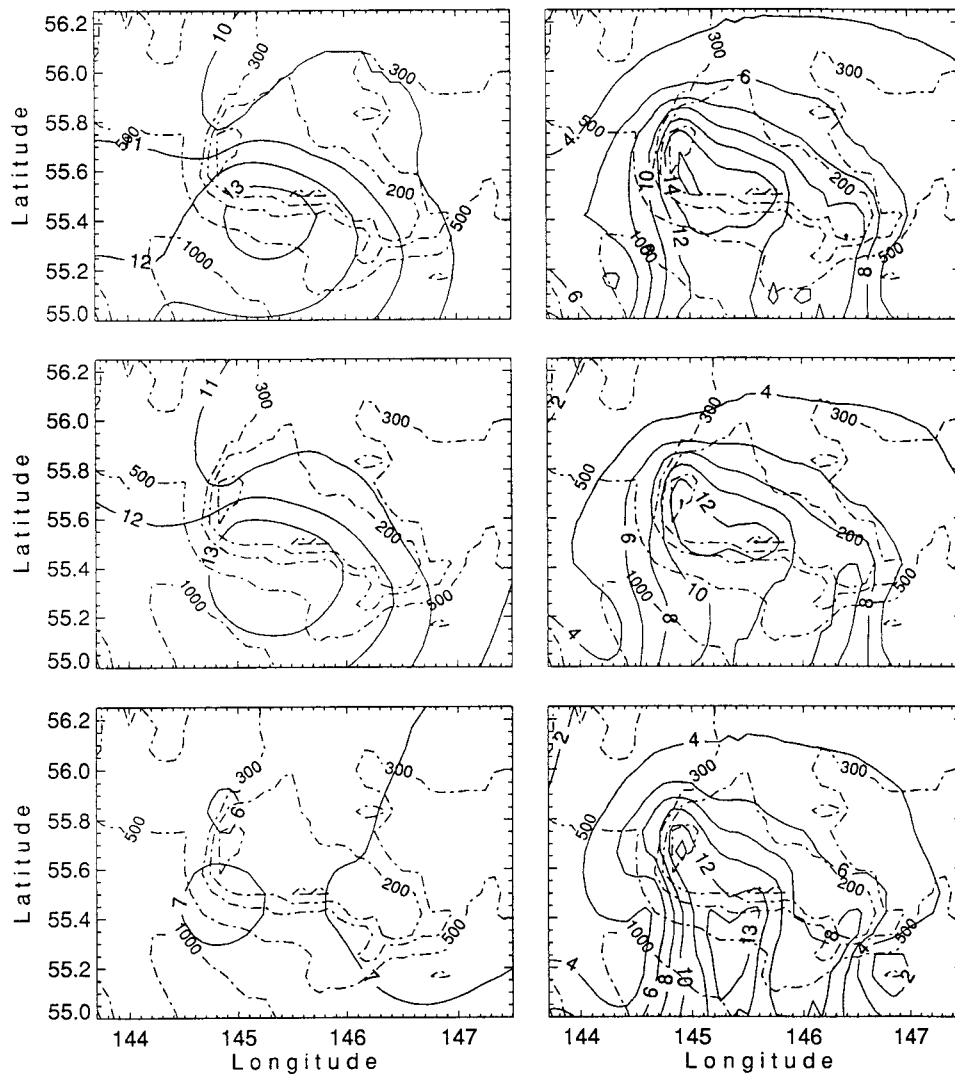


FIG. 16. Computed distribution of the amplification coefficients for sea level (left panels) and currents (right panels) for 26.3 h (top),  $O_1$  period (center), and  $K_1$  period (bottom) over Kashevarov Bank. Dot-dash lines depict bottom contours.

tom frictional terms do not transfer energy as effectively as advective terms. In summary, the nonlinear terms transfer energy from the  $K_1$  and  $O_1$  constituents toward longer and shorter periods. It can be deduced from Fig. 21 (center panel) that the energy from these waves mainly sustains oscillations in the fortnightly and semidiurnal bands. At the shorter periods, the magnitudes of energy maxima are very small.

The power spectra shed some light on the nature of the fortnightly periodicity, linking it to the advective accelerations. The time variations of the diurnal and fortnightly oscillations are reciprocally connected, which can be inferred through comparison of the top and the bottom panels in Fig. 18. There, larger  $K_1$  currents correspond to smaller fortnightly currents. The role of the bottom friction term in the fortnightly modulation of the  $K_1$  constituent depicted in Fig. 18 (top) cannot

be established explicitly. From Fig. 21 (bottom panel) it follows that nonlinear bottom friction does not generate 14-day oscillations. Therefore, bottom friction can only be an additional factor in  $K_1$  modulation if fortnightly oscillations are already present in the system due to advective acceleration.

## 5. Discussion and conclusions

A tidal model with 5' spatial resolution was applied to simulate tides in the Sea of Okhotsk. This rather high spatial resolution demonstrated peculiarities that were not previously disclosed by measurements or modeling studies. The results of the simulation show enhancement of the semidiurnal tidal amplitudes and currents in the shallow bays (Shelikhov Bay, Penzhinskaya, and Uds-kaya Guba of the Sea of Okhotsk and Tartar Bay of the

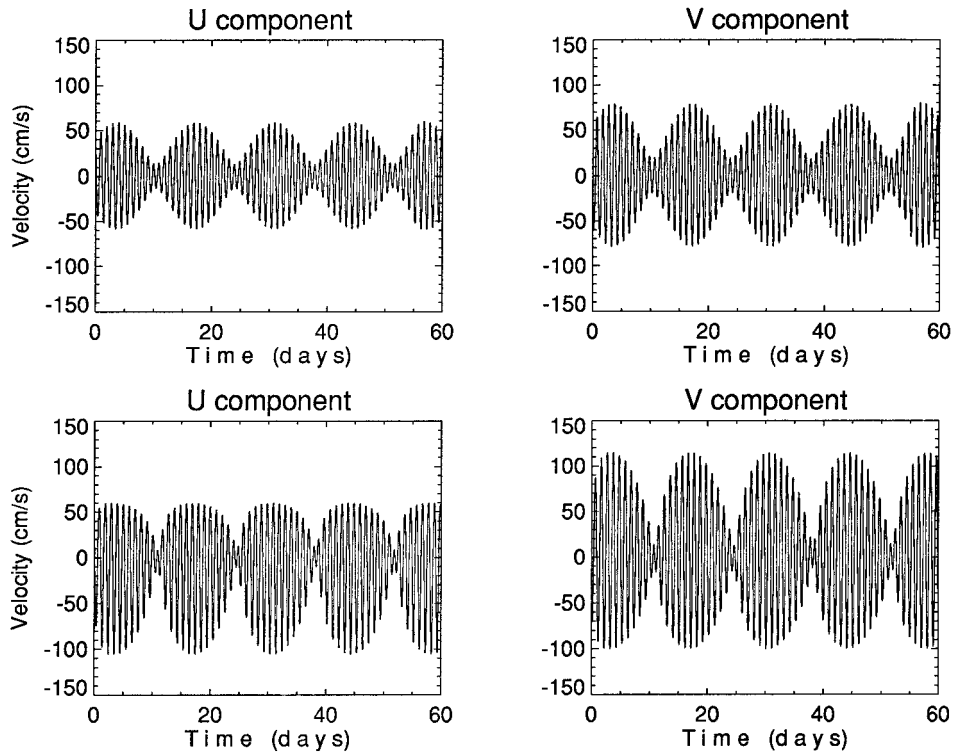


FIG. 17. Time series of the  $U$  (east-west) and  $V$  (south-north) components of tidal current at point P over Kashevarov Bank (see Fig. 14) for the linear (top) and nonlinear (bottom) simulations. Forcing is due to  $K_1 + O_1$ .

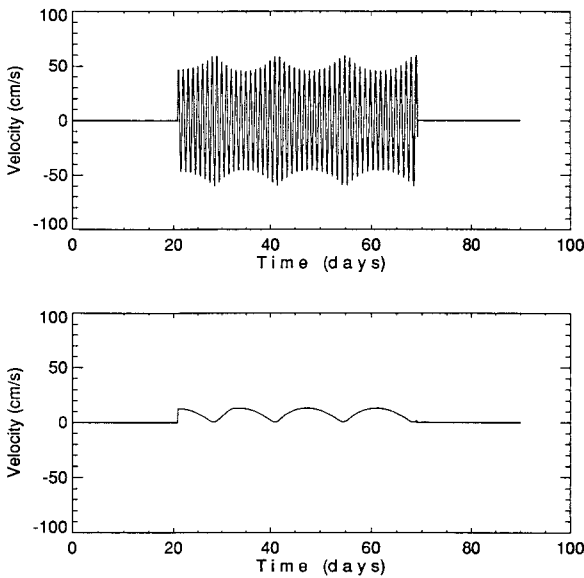


FIG. 18. Time series of the  $U$  (east-west) component of tidal current after filtration (at point P over Kashevarov Bank): (top)  $K_1$  wave period, (bottom) 13.66-day period and mean residual current. Forcing is due to  $K_1 + O_1$ .

Sea of Japan). Amplification of the diurnal amplitudes and currents is associated with the trapping of tidal energy by bottom irregularities like banks and steep slopes. The computation delineated strong diurnal currents at the eastern coast of Sakhalin, the northern coast of Hokkaido, the Kuril Islands, Kashevarov Bank, and the central Kamchatka coast.

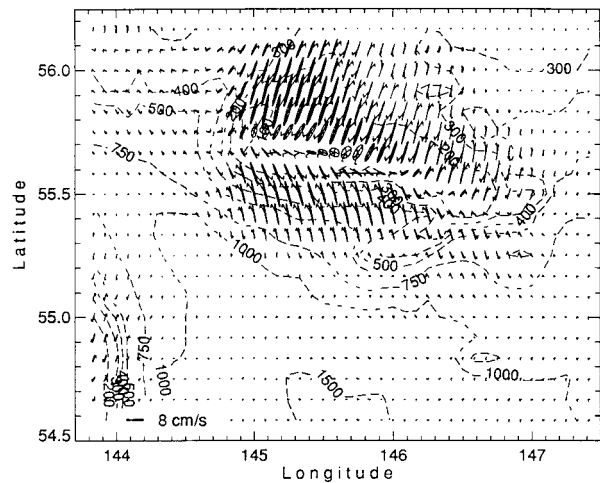


FIG. 19. Computed fortnightly tidal current ellipses. The arrow at each ellipse shows the direction of the current vector rotation. Dashed lines depict bottom contours.

Analysis of the energy budget in the Sea of Okhotsk showed that rather small areas may play an extremely important role in the dissipation of tidal energy. For example, in Shelikhov Bay and Penzhinskaya Guba the rate of energy dissipation of the diurnal tides is over 60% of the overall rate of energy dissipation of the diurnal tidal constituents in the entire Sea of Okhotsk. The total tidal energy dissipated in the Sea of Okhotsk is greater than the energy dissipated in the Arctic Ocean (Kowalik and Proshutinsky 1993). Thus, small water bodies can be significant sinks of tidal energy globally.

Investigations over Kashevarov Bank revealed enhanced diurnal tidal currents, a clockwise flux of tidal energy, and a local maximum in the magnitude of energy dissipation. The computed diurnal currents above the bank are approximately 10 times greater than the far-field values. Enhancement of diurnal tides over Kashevarov Bank is related to the near-resonant trapping of the tidal energy. This is due to the 26.3-h period that occurs in the free oscillation spectra both over Kashevarov Bank and in the entire SO. Detailed study of the natural oscillation spectra over Kashevarov Bank shows that the resonant amplification of velocity takes place over a wide range of periods.

Diurnal  $K_1$  and  $O_1$  currents, through the nonlinear interaction, generate new oscillations at semidiurnal  $M_2$  and fortnightly periods, and a residual current. An analogous phenomenon was observed at the Fieberling Guyot in the North Pacific (Brink 1995). The nonlinear interactions are studied by application of the filter. This line of research shows that the amplitude of the basic constituents ( $K_1$  and  $O_1$ ) is modulated by the fortnightly oscillations. The application of power spectra for investigation of  $K_1$  and  $O_1$  interactions over Kashevarov Bank indicates that the nonlinear terms transfer energy from the  $K_1$  and  $O_1$  tides toward longer and shorter periods. It can be deduced that the energy from these

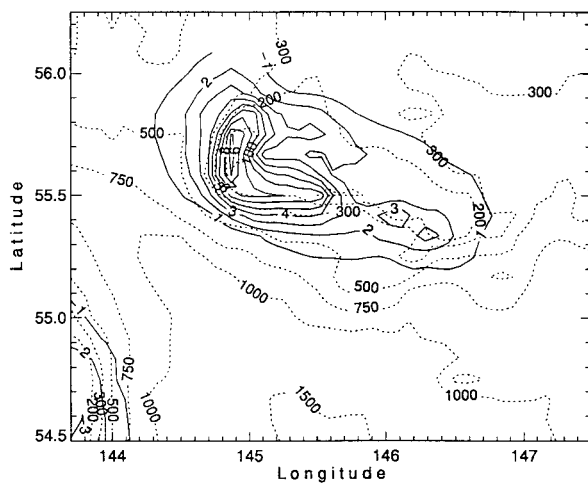


FIG. 20. Contours of the maximum  $M_2$  tidal current (solid lines,  $\text{cm s}^{-1}$ ) due to nonlinear interaction of the  $K_1$  and  $O_1$  constituents and depth contours (dotted lines, m) above Kashevarov Bank.

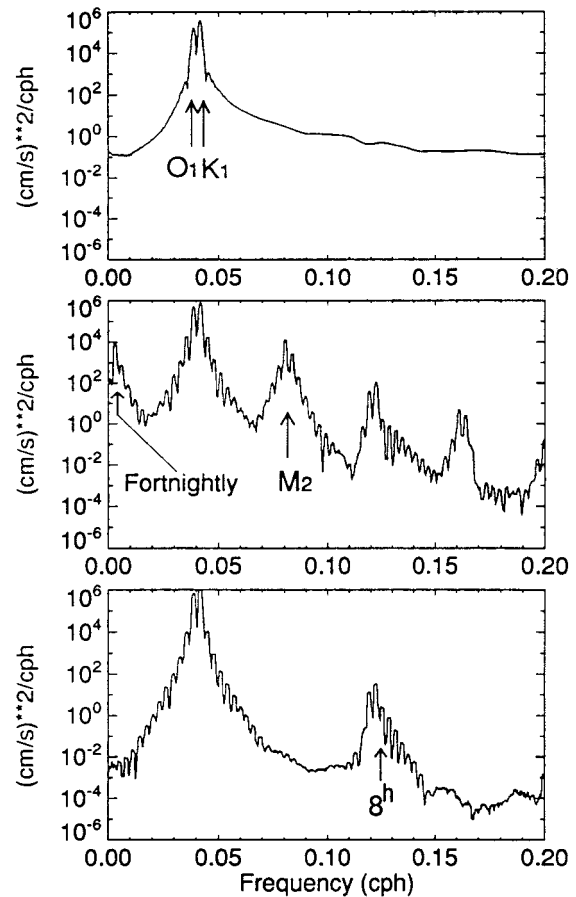


FIG. 21. Power spectra of the  $U$  (east-west) component of the tidal current at point P in Fig. 14. (top) Linear simulation, (center) fully nonlinear simulation, and (bottom) partly nonlinear simulation, due to the bottom friction. Forcing is due to  $K_1 + O_1$ .

constituents mainly sustains oscillations in fortnightly and semidiurnal bands. At the shorter periods the magnitude of energy maxima is very small.

*Acknowledgments.* We would like to express our gratitude to A. Yu. Proshutinsky from the Institute of Marine Science, University of Alaska, Fairbanks, for his help throughout the work. We are indebted to anonymous referees for the thoroughness of their comments and many improvements that strengthened the paper. Support of the Office of Naval Research under Grant N00014-95-1-0929 is gratefully acknowledged.

#### REFERENCES

- Alfultis, M. A., and S. Martin, 1987: Satellite passive microwave studies of the Sea of Okhotsk ice cover and its relations to oceanic processes, 1978–1982. *J. Geophys. Res.*, **92**, 13 013–13 028.
- Aota, M., and M. Matsuyama, 1987: Tidal current fluctuations in the Soya Current. *J. Oceanogr. Soc. Japan*, **43**, 276–282.
- Brink, K. H., 1989: The effect of stratification on seamount-trapped waves. *Deep-Sea Res.*, **36**, 825–844.

- , 1995: Tidal and lower frequency currents above Fieberling Guyot. *J. Geophys. Res.*, **100**, 10 817–10 832.
- Butman, B., M. Noble, D. C. Chapman, and R. C. Beardsley, 1983: An upper bound for the tidally rectified current at one location on the southern flank of Georges Bank. *J. Phys. Oceanogr.*, **13**, 1452–1460.
- Cartwright, D. E., R. D. Ray, and B. V. Sanchez, 1991: Oceanic tides maps and spherical harmonic coefficients from Geosat altimetry. NASA Tech. Memo. 104544, 75 pp.
- Chapman, D. C., 1983: On the influence of stratification and continental shelf and slope topography on the dispersion of subinertial coastally trapped waves. *J. Phys. Oceanogr.*, **13**, 1641–1652.
- , 1989: Enhanced subinertial diurnal tides over isolated topographic features. *Deep-Sea Res.*, **36**, 815–824.
- Clarke, A. J., 1991: The dynamics of barotropic tides over the continental shelf and slope. *Tidal Hydrodynamics*, B. B. Parker, Ed., Wiley and Sons, 79–108.
- Foreman, M. G. G., W. R. Crawford, and R. F. Madsen, 1995: Dettiding: Theory and practice. *Coastal and Estuarine Studies*, R. Lynch and A. M. Davies, Eds., Vol. 47, Amer. Geophys. Union, 203–239.
- Francis, O., and P. Mazzega, 1990: Global charts of ocean loading effects. *J. Geophys. Res.*, **95**(C7), 11 411–11 424.
- Gill, A. E., 1982: *Atmosphere-Ocean Dynamics*. Academic Press, 662 pp.
- Gladyshev, S. V., 1995: Fronts in the Kuril Islands region. *Oceanology*, **34**, 452–459.
- Haidvogel, D. B., A. Beckmann, D. C. Chapman, and R.-Q. Lin, 1993: Numerical simulation of flow around a toll isolated seamount. Part II: Resonant generation of trapped waves. *J. Phys. Oceanogr.*, **23**, 2373–2391.
- Hendershott, M. C., 1977: Numerical models of ocean tides. *The Sea*, Vol. 6, Wiley-Interscience, 47–96.
- Hunkins, K., 1986: Anomalous diurnal tidal currents on the Yermak Plateau. *J. Mar. Sci.*, **44**, 51–69.
- IDL Reference Guide, 1995: Interactive Data Language, version 4. Research Systems, Inc.
- Jeffreys, H., 1920: Tidal friction in shallow seas. *Philos. Trans. Roy. Soc. London*, **221**(8), 239–264.
- Kantha, L. H., 1995: Barotropic tides in the global oceans from nonlinear tidal model assimilating altimetric tides, 1. Model description and results. *J. Geophys. Res.*, **100**, 25 283–25 308.
- Kitani, K., and K. Shimazaki, 1971: On the hydrography of the northern part of the Okhotsk Sea in summer. *Bull. Fac. Fish. Hokkaido Univ.*, **12**(3), 231–242.
- Kowalik, Z., 1981: A study of the  $M_2$  tide in the ice-covered Arctic Ocean. *Model. Identif. Control*, **2**(4), 201–223.
- , 1994: Modeling of topographically amplified diurnal tides in the Nordic Seas. *J. Phys. Oceanogr.*, **24**, 1717–1731.
- , and A. Yu. Proshutinsky, 1993: Diurnal tides in the Arctic Ocean. *J. Geophys. Res.*, **98**, 16 449–16 468.
- Leonov, A. K., 1960: *Regional Oceanography* (in Russian). Gidrometeoizdat, Leningrad, 766 pp.
- LeProvost, C., M. L. Genco, and F. Lyard, 1994: Spectroscopy of the world ocean tides from a finite element hydrodynamical model. *J. Geophys. Res.*, **99**, 24 777–24 797.
- Lyard, F. M., and C. LeProvost, 1997: Energy budget of the tidal hydrodynamics model FES94.1. *Geophys. Res. Lett.*, **24**, 687–690.
- Marchuk, G. I., and B. A. Kagan, 1989: *Dynamics of Ocean Tides*. Kluwer Academic, 327 pp.
- Miller, G. R., 1966: The flux of tidal energy out of the deep ocean. *J. Geophys. Res.*, **71**, 2485–2489.
- Odamaki, M., 1994: Tides and tidal currents along the Okhotsk coast of Hokkaido. *J. Oceanogr. Soc. Japan*, **50**, 265–279.
- Parker, B. B., 1991: The relative importance of the various nonlinear mechanisms in a wide range of tidal interactions (Review). *Tidal Hydrodynamics*, B. B. Parker, Ed., Wiley and Sons, 237–268.
- Platzman, G. W., 1972: Two-dimensional free oscillations in natural basins. *J. Phys. Oceanogr.*, **2**, 117–138.
- Rabinovich, A. B., and A. Ye. Zhukov, 1984: Tidal oscillations on the shelf of Sakhalin Island. *Oceanology*, **24**(2), 184–189.
- Ray, R. D., and B. V. Sanchez, 1989: Radial deformation of the earth by oceanic tide loading. NASA Tech. Memo. 100743, 51 pp.
- Rogachev, K. A., A. S. Solomatin, V. I. Yusupov, and E. C. Carmack, 1996: On the internal structure of the Kuril Current Anticyclonic Rings. *Oceanology*, **36**, 347–354.
- Schwiderski, E. W., 1979: *Global Ocean Tides, Part II: The Semidiurnal Principal Lunar Tide ( $M_2$ )*. *Atlas of Tidal Charts and Maps*, Naval Surface Weapon Center, 87 pp.
- , 1981a–g: *Global Ocean Tides, Part III: The Semidiurnal Principal Solar Tide ( $S_2$ )*, 96 pp.; *Part IV: The Diurnal Luni-Solar Declination Tide ( $K_1$ )*, 87 pp.; *Part V: The Diurnal Principal Lunar Tide ( $O_1$ )*, 85 pp.; *Part VI: The Semidiurnal Elliptical Lunar Tide ( $N_2$ )*, 86 pp.; *Part VII: The Diurnal Principal Solar Tide ( $P_1$ )*, 86 pp.; *Part VIII: The Semidiurnal Luni-Solar Declination Tide ( $K_2$ )*, 86 pp.; *Part IX: The Diurnal Elliptical Lunar Tide ( $Q_1$ )*, 86 pp., *Atlas of Tidal Charts and Maps*. [Available from Naval Surface Weapon Center, Dahlgren, VA 22248.]
- Suzuki, K., and S. Kanari, 1986: Tidal simulation of the Sea of Okhotsk (in Japanese). *Kaiyo Kagaku*, **18**, 455–463.
- Yefimov, V. V., Ye. A. Kulikov, A. B. Rabinovich, and I. V. Fine, 1985: *Ocean Boundary Waves*. Gidrometeoizdat, Leningrad, 280 pp.